Partial Separation of an Azeotropic Mixture of Hydrogen Chloride and Water and Copper (II) Chloride Recovery for Optimization of the Copper-Chlorine Cycle

by

Matthew P. Lescisin

A Thesis Submitted in Partial Fulfillment of the Requirements for the Degree of

Master of Applied Science

in

The Faculty of Engineering and Applied Science

Mechanical Engineering

University of Ontario Institute of Technology

September 2017

Contents

Abstract

An atmospheric-pressure distillation system is designed and constructed to partially separate hydrochloric acid and water. The system concentrates $HCl_{(aq)}$ between the electrolyzer and hydrolysis steps of the Copper-Chlorine (Cu-Cl) cycle. Thus, the system partially recycles $HCl_{(aq)}$, thereby decreasing the total operating cost of the cycle. The separation is only partial, as the mixture is unable to cross the azeotrope with only a single pressure. The distillation system consists primarily of one packed distillation column, which employs heating tapes and thermocouples to achieve a desired axial temperature profile. The column can be operated in batch or continuous mode.

After performing physical distillation experiments, it is found that feeds less than azeotropic concentration are separated into $H_2O_{(l)}$ and highly-concentrated $HCl_{(aq)}$ (albeit at less than azeotropic concentration). Feeds greater than azeotropic concentration are not investigated as they are extremely corrosive (rich in HCl) and would likely destroy the apparatus. Corrosion product is prevalent in the bottoms product; it is a source of error that is partially mitigated by filtration.

No correlation is found between feed concentration and output concentration. That is, the distillate is $H_2O_{(l)}$ and the bottoms is $HCl_{(aq)}$ near azeotropic concentration; as long as the feed concentration is any value less than azeotropic. In other words, the degree of separation is found to be independent of the feed concentration, for feed concentrations less than azeotropic. The bottoms concentration varies from experiment to experiment, but does so randomly, likely the result of corrosion impurities affecting the calculation of its concentration.

A simulation of pressure-swing distillation (PSD) is also performed to help determine the feasibility of HCl-H_2O separation and the degree of separation. Furthermore, an investigation into metastability and its effect on the crystallization of $CuCl_2$ from $HCl_{(aq)}$ solutions is presented in Chapter 4.

Acknowledgments

Dr. K. Pope, Dr. M. A. Rosen and Dr. O. A. Jianu are very gratefully acknowledged for their advice and guidance throughout this project. The financial assistance of the Natural Sciences and Engineering Research Council of Canada (NSERC), Ontario Research Fund (ORF) and Canadian Nuclear Laboratories (CNL) is gratefully acknowledged.

List of Figures

List of Tables

Nomenclature

Quantities

a_p	Packing specific surface area, $m^2/m^3 = m^{-1}$
A	Corrosion exposure area, cm^2
Ar	Archimedes number, dimensionless
c	Molarity, mol/L
c_N	Concentration, g solute/100 g solvent
dc^*/dT	Temperature Coefficient of solubility, (g solute/100 g solvent)/K
d_e	Equivalent diameter of packing, m
dT/dt	Cooling rate, K/s
D	Molar flow rate of distillate, mol/h
D_V	Diffusivity of the vapour phase, m^2/s
g	Gravitational acceleration, 9.81 m/s^2
h	Molar enthalpy, J/mol
HETP	Height equivalent to a theoretical plate, m
HTU	Height of a transfer unit, m
ID	Column internal diameter (equivalent to Φ), cm
k	Thermal conductivity, W/(m·K)
k_N	Nucleation rate constant, dimensionless
K	K-value, dimensionless
K_V	Mass transfer coefficient of the vapour phase, 1/s
K_{sp}	Solubility product constant, dimensionless
l	Condenser length, m
L	Liquid molar flow rate, kmol/h
$\dot{L}$	Corrosion rate, mm/year
L_{reflux}	Molar flow rate of reflux, mol/h
m	Mass, g
$m_{pipe,\ initial}$	Initial pipe (i.e., column) mass, g
m_{lost}	Mass lost to corrosion, mg or g
$\dot{m}$	Mass flow rate, g/s

m_{eq}	Slope of the equilibrium line, dimensionless
m_N	Nucleation order, dimensionless
MM	Molar mass, g/mol
MSZW	Metastable zone width, K
n	Number of moles, dimensionless
N	Number of theoretical equilibrium stages, dimensionless
NTU	Number of transfer units, dimensionless
OD	Column external diameter, cm
P	Pressure, atm or kPa
q	Mole fraction of liquid in feed, mol/mol
Q	Molar heat transfer, J/mol
$\dot{Q}$	Rate of heat transfer, W
R	Ideal gas constant, 8.314 J/mol · K
Re	Reynolds number, dimensionless
R_{ha}	Ratio of molecular weights of hydrated to anhydrous components, dimensionless
t	Column molar heating time, s/mol
$t_{exposure}$	Corrosion exposure time, h
T	Temperature, ℃ or K
u	Superficial velocity, m/s
v	Volume, m^3
v_v	Vapor linear velocity, m/s
v_0	Flooding velocity of vapor, m/s
V	Vapor molar flow rate, kmol/h
w	Uncertainty, units depend on quantity in question
x	Mole fraction of a component in the liquid phase, mol/mol
y	Mole fraction of a component in vapor phase, mol/mol
y^*	Equilibrium mole fraction of a component in the vapor phase, mol/mol
z	Packed column height, m
Z_p	Height of each packed bed, m
$\Delta G°$	Difference in Gibbs free energy at reference state, kJ/kg
$\Delta H°$	Difference in enthalpy at reference state, kJ/kg
$\Delta S°$	Difference in entropy at reference state, kJ/kg · K

Greek Letters

α	Relative volatility, dimensionless
ε	Fractional voidage, m^3/m^3; Conversion factor, dimensionless
ν	Dynamic viscosity, Pa·s = kg/(m·s), or cP (1000 cP = 1 kg/(m·s))
ρ	Density, kg/m^3 or g/ml

ρ_{metal}	Column metal density, g/cm^3
σ	Molecular diameter, Å; Collision diameter, Å
σ_{L}	Surface tension, mN/m or N/m
Φ	Column internal diameter (equivalent to ID), m
ω	Interfacial surface area per unit volume of column, m^2/m^3
Ω	Molecular property, dimensionless, $\approx$1

Subscripts

aq	Aqueous state
b	Bottoms
d	Distillate
f	Feed
g	Gas phase
G	Gas state
i	Component *i*, (chemical species *i*)
l	Liquid phase
L	Liquid state
v	Vapor phase
V	Vapor state

Acronyms

ED	Extractive distillation
EES	Engineering Equation Solver (software)
HCl	Hydrogen Chloride
HPC	High-pressure column
LPC	Low-pressure column
PPAQ	Partial-Pressure of Aqueous Solutions (Thermodynamic model)
PSD	Pressure-swing distillation
SRK	Soave-Redlich-Kwong (Thermodynamic model)
TAC	Total annual cost
VLE	Vapor-liquid equilibrium

Chapter 1

Introduction

Alternative energy (e.g., solar, wind, hydrogen, geothermal) is of vital importance because the world's supply of fossil fuels is limited and the production/consumption of fossil fuels produces pollution. Hydrogen (H_2) is a promising alternative to fossil fuels because it does not produce CO_2 or other pollutants (e.g., CO, NO_x, SO_x), when used as an energy source. Since H_2 does not occur naturally, it must be produced by techniques such as steam-methane reforming. However, steam-methane reforming is disadvantageous because it requires natural gas, which is a fossil fuel, and because CO is produced as a byproduct [1].

The Copper-Chlorine (Cu-Cl) cycle is a novel 4-step thermochemical cycle to generate hydrogen, presented in Equations 1.1 to 1.4 [2] and Figure 1.1.

$$1\ \text{(Electrochemical)} : 2CuCl_{(aq)} + 2HCl_{(aq)} \rightarrow 2CuCl_{2(aq)} + H_{2(g)} \quad 25\,℃ - 90\,℃ \tag{1.1}$$

$$2\ \text{(Drying)} : 2CuCl_{2(aq)} \rightarrow 2CuCl_{2(s)} \quad 60\,℃ - 200\,℃ \tag{1.2}$$

$$3\ \text{(Hydrolysis)} : 2CuCl_{2(s)} + H_2O_{(g)} \leftrightarrow Cu_2OCl_{2(s)} + 2HCl_{(g)} \quad 350\,℃ - 450\,℃ \tag{1.3}$$

$$4\ \text{(Thermolysis)} : Cu_2OCl_{2(s)} \rightarrow 2CuCl_{(l)} + {}^1\!/_2\ O_{2(g)} \quad 520\,℃ \tag{1.4}$$

The $HCl_{(aq)}$ concentration step (which occurs between the hydrolysis step (step 3) and electrochemical step (step 1)) is not explicitly listed in [2], however, it may be expressed as:

$$HCl_{(aq)}\text{Concentration} : 2HCl_{(aq)} \rightarrow 2HCl_{(g)} + H_2O_{(g)} \quad 110\,℃ \tag{1.5}$$

HCl is in the aqueous state (negating the vapour pressure due to volatility) in Equation 1.1 because the reaction temperature is less than the boiling point of $HCl_{(aq)}$. HCl is in the gaseous state in Equation 1.3 because the reaction temperature is greater than the boiling point of $HCl_{(aq)}$.

In Equation 1.5, the separation of HCl and H_2O is assumed to be complete. Since all HCl is separated from H_2O, and the temperature is ~110℃, both HCl and H_2O would be in the gaseous state (since 110℃ is greater than the boiling points of both pure HCl and pure H_2O (at 1 atm pressure)). Therefore, the subscript g is written for both products in Equation 1.5 to indicate gaseous state.

However, if the HCl-H_2O separation described in Equation 1.5 is only partial, then the products would be: $HCl_{(aq)}$, $HCl_{(g)}$, and $H_2O_{(g)}$.

The Cu-Cl cycle is advantageous over other hydrogen production cycles because of its lower temperature requirements. Waste heat (an industrial byproduct) can be used to drive the reactions of the Cu-Cl cycle. Distillation is relevant to the Cu-Cl cycle as it increases the concentration of the $HCl_{(g)}$ produced in step 3, recycles it, and makes it suitable for use as a reactant in step 1.

Distillation can be used to concentrate hydrochloric acid $HCl_{(aq)}$ between the hydrolysis and electrolyzer steps of the Cu-Cl cycle as shown in Figure 1.1. HCl concentration (via distillation using waste heat) occurs at the location of the condenser/evaporator on Figure 1.1, $HCl_{(g)}$/steam $\rightarrow$ $HCl_{(aq)}$.

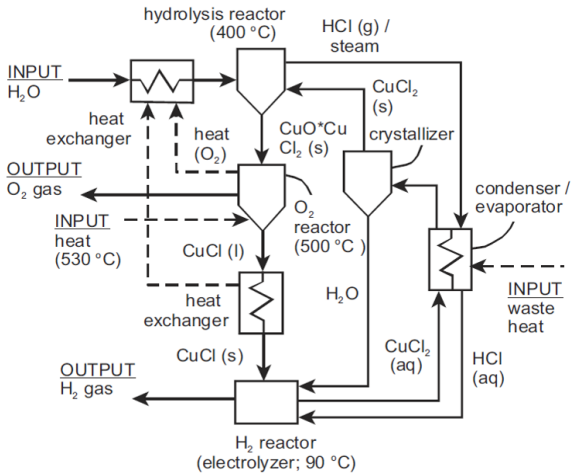

Figure 1.1: Schematic of the Cu-Cl cycle [2].

The problem addressed in this thesis, is recycling HCl within the Cu-Cl cycle, by separating HCl from water. Recycling HCl is needed to maintain the Cu-Cl cycle's efficiency. Therefore, an economical method of concentrating $HCl_{(aq)}$ is needed.

The objective of this thesis to demonstrate that the concentration of $HCl_{(aq)}$ can be increased (and thus a partial separation can be performed) using a single distillation column, provided that the feed concentration is less than azeotropic (0.11 mole fraction HCl).

The scope of this thesis comprises: a review of existing literature, simulation of distillation, design calculations, component and material selection, programming, column assembly, column operation, output analysis (e.g., determining the concentration of $HCl_{(aq)}$ in the output products) and the providing of recommendations. Work performed in this thesis for HCl-water separation includes: simulation, calculations, design, programming, construction, column operation and output analysis.

Optimization (e.g., increasing energy efficiency of the distillation column) falls outside the scope of this thesis, since the focus of this thesis is feasibility.

Other researchers, such as Fayazuddin [3], have used software to simulate a pressure-swing distillation system. However, to the author's knowledge, no documented attempt has been made to physically construct an HCl-water distillation system. Aghahosseini [4] concluded that pressure-swing distillation is not economical without heat-integration. Li et al. [5] performed an Aspen simulation for heat-integrated pressure-swing distillation (PSD) on an ethylenediamine/water system and found that the heat-integration decreases energy consumption by 19.79% and decreases total annual cost by 15.30%. The work of these and other researchers is detailed in Chapter 3.

The feasibility of separating HCl from water with reasonable purity (i.e., the feasibility of the separation from a chemical standpoint and from a construction standpoint) is determined using simulation software (Chapter 5) and design calculations (Chapter 6). Design calculations are made using analytical and empirical methods. One distillation column, operating at atmospheric pressure is built. A single-pressure column is adequate for the purpose of this thesis, because it produces pure HCl (but not pure water), provided the feed concentration of HCl is greater than the azeotropic concentration. The output of the column is analyzed using the techniques described in Section 6.3.

This thesis describes the the theoretical and experimental work performed for concentrating $HCl_{(aq)}$. The theoretical work includes a review of existing literature, a simulation of the system, and the calculation of column parameters (e.g., length, diameter, heat duty). Crystallization increases the energy efficiency of the Cu-Cl cycle because, in contrast to spray drying, it does not require a pump to force the mixture through a nozzle. Distillation reduces the operating cost of the Cu-Cl cycle by recycling $HCl_{(aq)}$.

Results are not consolidated, but rather presented in their corresponding section. This is done so that results may be presented alongside their context. Crystallization and metastability results are presented in Section 4.1, simulation results are presented in Section 5.3, and distillation experimental results are presented in Chapter 10.

Chapter 2

Background

2.1 Boiling in the Subcooled Liquid Region

Most liquids are partially vapourized when the temperature and pressure are in the subcooled liquid region (i.e., when the temperature is below the boiling temperature and the pressure is above the boiling pressure). This partial vapourization is caused by an unequal distribution of molecular kinetic energies in a specimen of uniform temperature. Temperature is the *average* kinetic energy of molecules; the standard deviation of molecular kinetic energies can be quite large. Some molecules have sufficient kinetic energy to overcome the intermolecular bonds (intermolecular forces) that hold them in the liquid state, and consequently enter the gaseous (vapour) state. Hence, the liquid has a vapour (of the same chemical formula) above it even though the temperature and pressure are in the subcooled liquid region. The vapour phase above the liquid phase exerts a pressure, known as *vapour pressure*.

It is due to the unequal distribution of molecular kinetic energies in a specimen of uniform temperature (resulting in some molecules having sufficient kinetic energy to overcome the intermolecular forces which hold them in the liquid state and enter the vapour state), that water at room temperature gradually evaporates.

The notion of a subcooled liquid region (i.e., only liquid and no vapour if the temperature is below the boiling temperature and the pressure is above the boiling pressure) belongs to an idealized thermodynamic model which assumes that each and every molecule in a specimen of uniform temperature has identical kinetic energy. This thermodynamic model is useful in many contexts, but it cannot be used to describe distillation.

2.2 Vapor-Liquid Equilibrium (VLE)

Different chemical species have different standard deviations of molecular kinetic energy for the same temperature. Those which have a larger fraction of molecular kinetic energies in the gaseous state (i.e., above a certain threshold), at a given temperature, exert a higher *vapour pressure*.

The greater the vapour pressure exerted by a given chemical species at a given temperature, the greater the *volaltility*. Liquid chemical species which exert a vapour pressure (most of them) are said to be *volatile*. The K-value for component i, K_i, is the ratio of the mole fraction in the vapour phase ($\mathrm{y_i}$) to the mole fraction in the liquid phase ($\mathrm{x_i}$).

$$K_i = \frac{y_i}{x_i} \tag{2.1}$$

If the temperature and chemical composition are held constant, then the rates of vapourization and condensation are equal and the substance is said to be in *vapour-liquid equilibrium* (VLE), which is a type of dynamic equilibrium.

For a mixture of n components (i.e., chemical species), the total vapour pressure (above the mixture) is the sum of the vapour pressures of each component, as stated by Dalton's Law of Partial Pressures (Equation 2.2):

$$P_{total} = \sum_{i=1}^{n} P_i = P_1 + P_2 + ... + P_n \tag{2.2}$$

2.3 Phase Diagrams

Concentration is conventionally expressed as the mole fraction of the more volatile component, as shown by Equation 2.3 (either as number between 0 and 1, or as a percentage).

$$Mole\ Fraction = \frac{Moles\ of\ the\ more\ volalitle\ component\ in\ a\ certain\ phase}{Total\ moles\ in\ that\ same\ phase} \tag{2.3}$$

A phase diagram (Figure 2.1) shows the dew point temperature (when the vapour begins to condense (upper curve)) and bubble point temperature (when the liquid begins to boil (lower curve)) for binary mixture, as a function of concentration. In the region between the curves, vapour and liquid exist simultaneously in VLE.

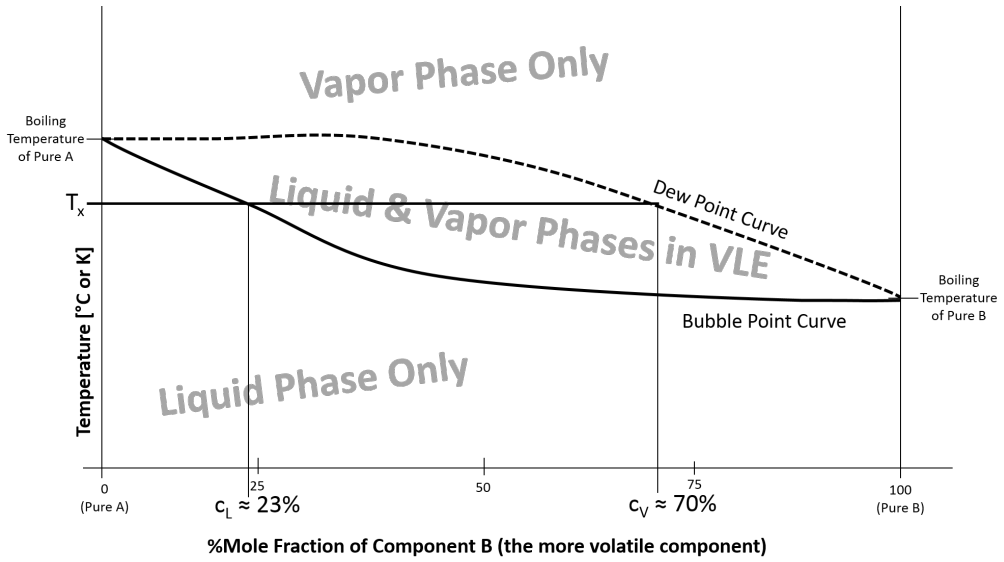

Figure 2.1: Phase diagram for a fictitious binary mixture of A and B, where B is the more volatile component.

2.3.1 Tie-Lines

For a given temperature, the concentration (of the more volatile component) in the vapour and liquid phases can be found via the tie-line method. The method consists of drawing a horizontal line at the desired temperature, then reading the horizontal coordinate (i.e., concentration) of the point where it intersects the bubble point curve (liquid concentration) and the dew point curve (vapour concentration).

Figure 2.1 shows the tie-line (horizontal line at T_x), vapour concentration c_V, and liquid concentration c_L, for a temperature T_x.

2.4 Distillation

Distillation is the separation of two or more chemical species based on vapour pressure, boiling points and relative volatility.

In order for distillation to be feasible, the vapour pressure (and consequently y) of each component must be different, in a mixture of uniform temperature. For example, for a mixture of HCl and H_2O at room temperature, HCl exerts a larger vapour pressure and consequently has a larger y. Symbolically, this is: @ $T_{room} : y_{HCl} > y_{H_2O}, P_{HCl} > P_{H_2O}$.

The greater the difference in y for two components, the greater the relative volatility, α. A greater α means that fewer equilibrium stages are required to achieve a given

separation (a given purity). The relative volatility for two components, i and j, can also be expressed as the ratio of their K-values. Usually, the larger K-value is written in the numerator, such that $\alpha \geq 1$.

$$\alpha_{ij} = \frac{K_i}{K_j} = \frac{y_i/x_i}{y_j/x_j} \tag{2.4}$$

For a component i, in a mixture, y_i increases with temperature. y_i and K_i increase with temperature, whereas x_i decreases with temperature. A different vapour-liquid equilibrium exists at a different temperature. For this reason, temperature varies from stage to stage along the length of a distillation column. Typically, temperature is highest at the bottom of the column and decreases with height.

In distillation, the vapour of a certain concentration (usually expressed as mole fraction of the more volatile component) at given stage (or theoretical plate) rises due to buoyancy and due to the slight pressure differential along the column height. The bottom of the column is usually hottest so that it will be at the highest pressure. This temperature differential creates a corresponding pressure differential which helps the vapour phase rise to the next stage. When the vapour travels upward and reaches the next stage, which is colder than the stage below it, the vapour partially condenses to a liquid of the same concentration. At this new temperature there is still vapour above the liquid (i.e., VLE is occuring). However, the vapour at the new stage is at a different concentration than the vapour at the previous stage. This vapour also rises to the next stage and condenses. In this way, as shown in Figure 2.2, separation is achieved.

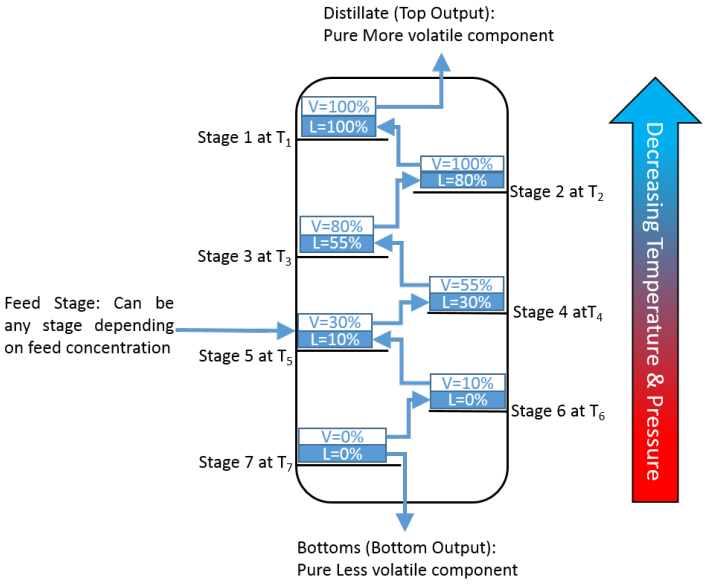

Figure 2.2: Distillation column with 7 stages for a fictitious binary mixture.

In Figure 2.2, the concentrations of vapour (V) and liquid (L) are expressed in percentages as mole fractions of the more volatile component. For example, at the feed stage (stage 5): $V_{\text{more volatile}} = 30\%$
$\therefore V_{\text{less volatile}} = 100\%$ - $30\% = 70\%$, and
$L_{\text{more volatile}} = 10\% \therefore L_{\text{less volatile}} = 100\%$ - $10\% = 90\%$.

2.5 Azeotropes

An azeotrope occurs when the concentration of the vapour and liquid phase are equal, thus making further separation by typical distillation techniques impossible. Therefore, an azeotrope only occurs at a certain concentration (i.e., the azeotropic concentration). At other concentrations, no azeotrope is present. The azeotropic concentration may vary with pressure. On a phase diagram, an azeotrope is indicated by the dew point and bubble point curves touching.

Not all mixtures have azeotropes, however HCl-H_2O has an azeotrope at about 11.1% mole fraction HCl at a pressure of 1 atm [6].

Chapter 3

Literature Review

The purpose of the literature review is to obtain a thorough understanding of what has already been accomplished in field of pressure-swing distillation (especially how it pertains the Cu-Cl cycle). Topics examined include: azeotropic distillation, extractive distillation, pressure-swing distillation, batch mode, heat-integration distillation columns, reflux ratio and HETP (height equivalent to a theoretical plate) correlations.

A significant portion of the research cited in the literature review does not directly pertain to HCl-water separation, however, it is still relevant, as the principles (pressure-swing distillation, heat) and outcomes (lower TAC (total annual cost), energy savings, higher purities, etc.) detailed therein are applicable to azeotropic HCl-water systems.

Although the Cu-Cl Cycle requires the separation of a binary mixture (namely HCl-water), the sources in this review are useful as they provide insight into heat integration which results in considerable energy savings.

3.1 Azeotropic Distillation

Azeotropic distillation of chemical species A and B requires an entrainer, E, which forms another azeotrope with either A or B. In the first column, E is mixed with A + B. Pure A is separated from the resulting azeotropic mixture B + E. Pure A exits via the bottom and B + E exits via the top and flows into a decanter. In the decanter, two insoluble liquid layers occur; one rich in B, the other rich in E. The layer rich in E returns to the first column, and the layer rich in B travels to the second column where some pure B is separated from the azeotropic mixture B + E. Pure B exits via the bottom and B + E exits via the top and returns to the decanter [7].

An example of azeotropic distillation to separate water and acetic acid with ester as the entrainer is given in Figure 3.1 [7].

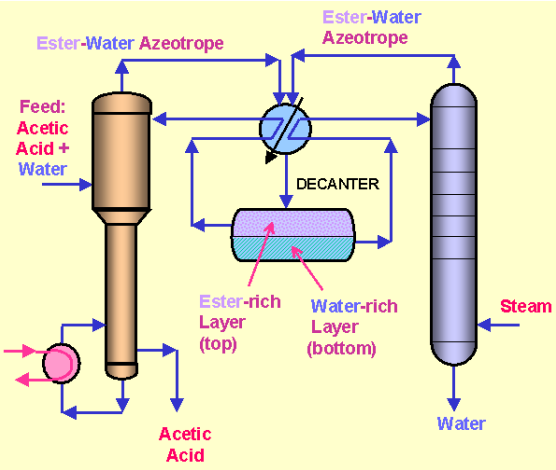

Figure 3.1: Azeotropic Distillation Example [7]

In azeotropic distillation, it is imperative that a suitable entrainer is selected. A suitable entrainer is one that allows the formation of the *insoluble* liquid layers, since insolubility is necessary for successful separation. That is, one of the chemical species to be separated must be insoluble in the entrainer.

Knapp and Doherty [8] discuss conventional pressure-swing distillation (PSD) for pressure-sensitive (where the azeotropic concentration changes with pressure) binary azeotropes, such as HCl-water, which resembles that encountered in the Cu-Cl cycle. PSD for ternary mixtures as well as a new PSD process for pressure-insensitive azeotropes which requires an entrainer to create a pressure-sensitive azeotrope, are discussed. Chien et al. [9] investigated azeotropic distillation of an isopropyl alcohol (IPA)-water system with use of cyclohexane (CyH) as an entrainer. A 2-column and 3-column method are compared. It is concluded that the 2-column method is less costly.

3.2 Extractive Distillation

Extractive distillation, which separates a close-boiling binary mixture of A & B, requires a solvent with a boiling point substantially higher than those of both A and B. A and B must both be soluble in the solvent. The solvent breaks the azeotrope because it changes the relative volatility of A to B [10]. In the first column, A is separated from the solution of B and the solvent. The solution of B and the solvent is then pumped to the second column, in which B is separated from the solvent. Finally, the recovered solvent is returned to the first column. The solvent used in extractive distillation must be completely removed in each column so that purity is not affected.

Although similar to azeotropic distillation, extractive distillation is simpler in most

cases. This is because extractive distillation breaks the azeotrope (whereas azeotropic distillation does not), and extractive requires less apparatus (e.g., azeotropic distillation requires a decanter whereas extractive distillation does not).

Numerous researchers [11–14] have found PSD to have a lower cost than extractive distillation. This is probably because extractive distillation requires the use and extraction of a solvent, which adds more components, steps and apparatus to the separation system. However, other researchers [15, 16] have found extractive distillation to have the lower cost. Since the researchers cited used different chemicals (that variable is uncontrolled), it is also evident that the chemicals to be separated play a major role in the cost.

Luyben [15] investigated PSD and extractive distillation for a maximum-boiling azeotrope of acetone and choloroform. It is concluded that PSD has a TAC of $4,327,000, whereas extractive distillation has a substantially lower TAC of $952,700. Luyben [16] compared extractive distillation and PSD for an acetone-methanol system. The extractive system was found to have 15% lower TAC. Wang et al. [11] compared extractive distillation and PSD for a tetrahydrofuran (THF)-ethanol system. They found that PSD is more economical (contrary to [16], although different chemicals are used) and also gives higher purities of the outputs. The capital costs of PSD and extractive distillation, are $\$0.9310 \times 10^6$ and $\$0.9450 \times 10^6$, respectively. Muñoz et al. [12] performed a simulation with Aspen HYSYS to compare the separation of a system 12,000 Tm/year of 52 mole% isobutyl alcohol and 48 mole% isobutyl acetate, via extractive distillation (with n-butyl propionate as an entrainer), and via PSD. They concluded PSD has a lower TAC than extractive distillation (1.123×10^6 USD/year and 1.508×10^6 USD/year, respectively). It is also concluded that PSD has lower fixed capital investment than extractive distillation (2.492×10^6 USD and 3.924×10^6 USD, respectively). Lladosa et al. [13] compared PSD and extractive distillation (ED) for a mixture of 50 mol% di-n-propyl ether and 50 mol% n-propyl alcohol, using Aspen HYSYS. It is found that PSD has a substantially lower fixed capital investment (1.205×10^6 USD and 1.925×10^6 USD, for PSD & ED (extractive distillation), respectively), as well as lower TAC (514.99×10^3USD/year and 730.13×10^3 USD/year, for PSD & ED, respectively), compared to extractive distillation. Hosgor et al. [14] performed a comparison between extractive distillation and PSD (with and without heat integration) on a simulated system of methanol-chloroform in Aspen Plus and Aspen Dynamics. They found PSD (TAC = 0.7269×10^6\$/yr) to be less costly than extractive distillation (TAC = 2.2174×10^6\$/yr).

3.3 Pressure-Swing Distillation

QVF Corporation [17] investigated Dual-Pressure Distillation (i.e., pressure-swing distillation (PSD)) for HCl-water systems. A plot of azeotropic HCl concentration as a

function of pressure shows that azeotropic concentration decreases with pressure. Such data is vital for selecting the PSD pressures. A process flow diagram of a proposed PSD system is also provided. Fayazuddin [3] investigated PSD of HCl-water systems for the Cu-Cl cycle for hydrogen production using simulations in CHEMCAD software. PSD is found to be less costly than azeotropic distillation since no entrainer is required. At pressures of 1 atm and 20 atm, an HCl purity of 80.4% is obtained. At pressures of 0.1 atm and 10 atm, an HCl purity of 76.6% is obtained. Aghahosseini [4] investigated azeotropic mixture separation for HCl-water systems, including PSD. It was concluded that PSD is not economically viable without heat exchange between the high-pressure (hotter) column and low-pressure (colder) column. Aghahosseini [4] also investigated other methods for azeotropic separation such as extractive distillation and concluded that for extractive distillation, the reflux flow rate should be minimized as excessive reflux dilutes the entrainer, thereby decreasing its effectiveness. Palomino et al. [18] investigated PSD for an ethanol-water system. First, the concentration of ethanol was increased from 80% v/v to 95% v/v, using simple distillation. Then the concentration of ethanol was increased from 95% v/v to 97% v/v via PSD. Wang et al. [19] examined a system of n-heptane and isobutanol which forms both minimum- and maximum-boiling azeotropes, depending on pressure. The LPC is set at atmospheric pressure, which results in two different PSD processes: conventional PSD (CPSD) and unusual PSD (UPSD). CPSD forms minimum-boiling azeotropes under both low and high pressures. UPSD forms minimum-boiling azeotropes under low pressure and maximum-boiling azeotropes under high pressure. It is concluded that CPSD has a lower TAC than UPSD, whereas UPSD has better dynamic control than CPSD. Fulgueras et al. [20] performed a simulation to separate ethylenediamine (EDA) from aqueous solution using PSD with heat integration for low-high (LP+HP) and high-low (HP+LP) configurations. The minimum number of column stages is achieved when the low and high pressures are 100 mmHg and 4909.6 mmHg, respectively.

Phimister and Seider [21] discuss PSD using only one column, which is alternated between the low and high pressures (known as semi-continuous PSD). According to [21], cost savings can be achieved by using one column with alternating pressures. A simulation is performed for a tetrahydrofuran-water system. It is concluded that the cost decreases by 22.5% - 32.5% when semi-continuous PSD (single-column) is used. However, with semi-continuous PSD one must use larger feed tanks, perhaps a more complex control system and also heat cannot be transferred between columns. These constraints diminish the cost savings.

3.4 Batch Mode

A unit operation (such as distillation) may be operated in batch mode (discrete) or continuous mode. In batch mode, an amount feed is input to the column, and no more feed is added until the initial amount is processed. In continuous mode, at steady-state, the sum of the mass flow rates into and out of the unit are constant. An advantage of batch mode is usually lower capital cost, because a feed pump is not required as the feed can be input manually at the beginning of each batch.

Modla and Lang [22] examined batch PSD methods such as: rectifier, stripper, and middle vessel column. Two new configurations are proposed: double column batch rectifier (DCBR) and double column batch stripper (DCBS). DCBR and DCBS are found to be advantageous over the preexisting configurations, due to the presence of only one production step, no change in pressure, almost steady-state operation of both column section, and thermal integration of the columns. Repke et al. [23] investigated batch PSD for an acetonitrile-water system, using two modes of batch PSD; regular and inverted. The inverted batch mode is found to require less time per batch than the regular mode, for feeds with a small amount of light (low-density) component.

3.5 Heat-Integrated Distillation Columns

Heat-integration is employed in distillation systems (PSD and other types) to reduce energy consumption and TAC. Generally, heat integration consists of a heat exchanger which transfers heat from an output of one column to an input of another column. Heat integration increases the capital cost (because of the extra components, namely, the heat exchanger and accessories). However, the researchers [24–28] found that heat-integration decreases the TAC since less external heat is required.

Kiss and Olujic [24] investigated internally heat-integrated distillation columns (HIDiC), which can be used for simple distillation, as well as PSD. It is found that a HIDiC can realize a maximum of 70% energy savings over conventional distillation columns. Shahandeh et al. [25] performed a comparison between: HIDiC (Heat-Integrated Distillation Column), VRC (Vapor Recompression Column) and CDiC (Conventional Distillation Column). The comparison is performed on three mixtures: benzene-toluene, propane-propylene and methanol-water. The comparison is performed in terms of TAC (total annual cost). It is found that a CDiC is optimal for benzene-toluene, a VRC is optimal for propane-propylene (44.1% decrease in TAC relative to CDiC), and a HIDiC is optimal for methanol-water (3.4% decrease in TAC relative to CDiC, and 31.2% decrease in TAC relative to VRC). Ponce et al. [26] used Aspen Plus to compare the energy requirements for a HIDiC ((heat-integrated distillation column) with and without heat

panels) and a CDiC (Convential Distillation Column), for the separation of an ethanol-water mixture. Energy savings of approximately 77% in the boiler, are obtained, relative to a CDiC when using a HIDiC with heat panels. Kiran and Jana [27] propose a PSD system which incorporates both HIDiC (heat-integrated distillation column) and VRC (vapour recompression column), to increase the energy efficiency of the system. The VRC ensures that the temperature of the vapour in the HPC is at least 20 K hotter (minimum difference in temperature) than the LPC. The combined HIDiC-VRC system has energy savings of approx. 29.5%, when simulated for a system of ethylacetate. Mulia-Soto et al. [28] simulated PSD with internal heat integration (IHIPSD) for separation of an ethanol/water mixture. Using internally heat integrated PSD (IHIPSD), the total heat input was reduced from 6.33 MW to 4.30 MW. The LPC is at 1 atm and the HPC is at 10 atm.

3.5.1 Heat-Integrated PSD

Heat integration is especially benefical when combined with PSD, as it takes advantage of the temperature rise that occurs when the fluid is pressurized, by routing the resulting excess heat (that would otherwise dissipate to the surroundings) from the HPC to LPC. Typically, heat integration consists of a heat exchanger which transfers heat from one of the HPC outputs to one of the LPC inputs. As the pressure of the HPC output drops through the adiabatic heat exchanger, the fluid expands and cools, thus transferring heat to the LPC input and decreasing the reboiler duty of the LPC. Similar to Section 3.5, heat integrated PSD is found to increase the capital cost (because of the extra components, namely, the heat exchanger and accessories), but is also found to decreases the TAC and energy consumption since less external heat is required.

Abu-Eishah and Luyban [29] investigated energy consumption reduction of PSD for a tetrahydrofuran-water system. Heat integration and feed preheat were employed to decrease the energy consumption by approximately half. Cheng and Luyben [30] investigated heat integration for a ternary system of benzene-toluene-m-xylene and realized energy savings of 35%-45% depending on configuration. Li et al. [5] used Aspen Plus and Aspen Dynamics to simulate a partially heat-integrated pressure-swing distillation process for separating an ethylenediamine/water system. Partially heat-integrated PSD was found to decrease energy consumption by 19.79% and decreases TAC by 15.30%. Kiran and Jana [31] discuss heat integration for PSD of bioethanol dehydration. Three methods are compared: 1.) only heat integrated distillation column (HIDiC), 2.) ideal hybrid HIDiC-VRC (Vapor Recompression Column, and 3.) conventional standalone PSD. The ideal hybrid HIDiC-VRC is found to be the optimal solution, with energy savings of 82.88% and TAC savings of 22.16%.

3.6 Reflux Ratio

Reflux ratio is the ratio of the amount product re-entering the column to the amount of product leaving the top of the column as distillate. The use of reflux is not mandatory, however, a higher reflux ratio tends to result in a higher purity of the distillate as it passes through the column several times before finally leaving.

Knapp [32] discusses reflux ratio, which is the ratio of the amount of reflux (condensed liquid from the vapour ("tops")) that goes back down the column over the amount of reflux which leaves the column as distillate. Higher reflux ratios typically yield higher purity, but require more time to process a unit mass, since the net flow rate is lower (net flow = total - reflux). Maximum reflux is the reflux above which separation is impossible. Lee et al. [33] performed a simulation, using PRO/II with PROVISION release 8.3, of PSD to separate a mixture of tetrahydrofuran (THF) and water. They found a reflux ratio of 0.4 on both columns resulted in lowest reboiler duty, presumably saving energy. They achieved purities of 99.9 mole% for both THF and water. Although, one should remember that these purities are the result of simulations, real-world purities are likely lower.

3.7 HETP Correlations

The work of Wang et al. [34] includes an aggregation of empirical HETP correlations for packed columns from numerous researchers. These correlations give HETP in terms of various parameters such as phase densities, phase velocities, phase dynamic viscosities and column diameter. The column height (z) is calculated in terms of HETP using Equation 7.1. These correlations and the results generated by them are given in Section 7.2.2.

3.8 Outcome of the Literature Review

After performing the literature review, it is determined that although simulations exist [3], no pressure-swing distillation to separate HCl-water has been physically performed. Therefore, it is decided that the focus of this research is to separate HCl-water via distillation. It is determined to avoid azeotropic distillation (using an entrainer and a decanter) and extractive distillation (using an additional solvent to break the azeotrope), as they require additional chemical species, additional separation step(s), and in the case of azeotropic distillation; additional apparatus (namely the decanter), all of which increases cost and complexity.

It is also determined to avoid the use of heat-integration because, although it results in energy savings and lower TAC in the long-term, it also increases the capital cost of the system (primarily due to the heat exchanger and associated piping). Since the system detailed in this thesis is of lab scale (and therefore is only used short-term, so decreasing capital cost is the priority), it is not economically viable to employ heat-integration.

Chapter 4

The Effect of Metastability on Crystallization

Crystallization is necessary for the integration of the hydrolysis and electrolyzer units of the Cu-Cl cycle for hydrogen production. As shown by Figure 1.1, crystallization is employed in the drying step of the Cu-Cl cycle to separate $CuCl_2$ and water according to:

$$CuCl_{2(aq)} \rightarrow CuCl_{2(s)} + H_2O_{(l)} \tag{4.1}$$

$CuCl_{2(s)}$ travels to the hydrolysis reactor and $H_2O_{(l)}$ travels to the electrolyzer, where they are inputs for their respective units. Crystallization is less energy intensive than other methods to recover solids from solution, such as spray-drying, which requires a pump to spray pressurized solution through a nozzle. Precipitation (of solids from liquid solutions) relies on the fact that the solubility of a solute in a liquid solvent increases with temperature. Since crystallization is the only form of precipitation discussed in this chapter, the words crystallization and precipitation are used interchangeably.

In one set of experiments, performed at UOIT's Clean Energy Research Laboratory, the solvent is heated to the high temperature, and the solute is added such that the concentration at the high temperature is greater than the saturation concentration at the low temperature. Upon cooling to the low temperature, the excess solute solidifies in the form of crystals.

Another set of experiments, also performed at UOIT's Clean Energy Research Laboratory, shows that the dissolution temperature (T_d) and the crystallization temperature (T_{met}) are not identical; the difference between them is the Metastable Zone Width (MSZW). This type of hysteresis is known as metastability. An understanding of metastability, described in Section 4.2, is used to optimize and refine the crystallization process.

4.1 Crystallization Results and Discussion

It is found that crystallization of $CuCl_2$ does not occur at HCl concentrations > 9M. Chemicals are added in the following order: water, $CuCl_2$, $HCl_{(aq)}$. Adding $HCl_{(aq)}$, despite there being negligible change in ambient temperature (e.g., negligible change in temperature due to enthalpy of mixing), causes crystallization to begin immediately. This is maybe due to $CuCl_2$ reacting with HCl to form complexes [35]. Anhydrous copper (II) chloride is found to never crystallize from $HCl_{(aq)}$ solutions. There is also a relatively narrow range of concentrations for which $CuCl_2$ will crystallize; if the concentration is below the range there will be no crystallization and the solution will remain liquid. Conversely, if the concentration exceeds the upper bound of the range, the solution will be saturated, and there will be precipitate at all temperatures in the range. The results of the crystallization experiments are summarized in Table B.1. The volume of the solvent ($HCl_{(aq)}$) is 100 mL.

There is a narrow range of concentrations that will demonstrate crystallization. If the initial concentration exceeds the upper bound of this range, the solution will be saturated and precipitation will occur instantly. Conversely, if the initial concentrations falls below the lower bound of this range, the solution will remain liquid upon cooling. It is found that anhydrous copper (II) chloride does not crystallize, crystallization does not occur at concentrations > 9M, and HCl can cause near-instantaneous crystallization when it is added to aqueous $CuCl_2$ solution.

Crystallization is achieved frequently and consistently when the solution temperature drops below the saturation temperature. As more experiments are performed, the success rate increased. However, further experiments should be performed to confirm the results and rule out the possibility of random, uncontrollable variables (e.g., chemical impurities, temperature fluctuations) causing or inhibiting crystallization. In the most recent experiments, the crystallized solid is collected via filtration and weighed upon completion; the delta (i.e., the mass of solute that remains dissolved, delta = $m_{solvent}$ - $m_{crystallized\ solid}$) will be compared against the values given in the solubility table.

4.2 Metastability

Metastability of $CuCl_2$ in H_2O-HCl for applications to the Cu-Cl thermochemical cycle is experimentally investigated to decrease crystallizing (precipitating) temperature and reduce thermal energy requirements of the cycle. Metastability delays the phase transition by altering the phase transition temperature, depending on direction of temperature change (i.e., heating or cooling). The dissolving temperature is increased if the solution is heated, and decreased if the solution is cooled. By contrast, a typical simple solubility

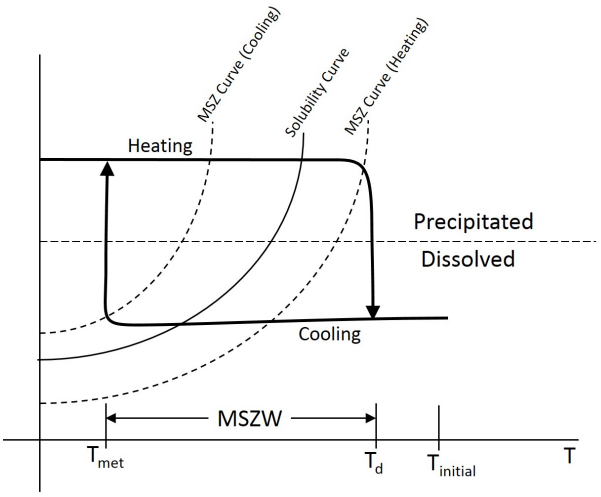

Figure 4.1: Hysteresis Loop of Metastability.

model assumes dissolution and crystallization occur at the same temperature. The solution temperature is controlled using an ethylene-glycol heater / chiller and measured via thermocouple. It is observed that the metastable zone width (MSZW) increases with cooling rate and is unaffected by HCl concentration. The solubility product constant (K_{sp}) is calculated for $CuCl_2$ dissolving in various concentrations of HCl and is found to decrease with temperature and with HCl concentration.

Crystallization is a promising method to recover solids in the Cu-Cl cycle for hydrogen production during the drying step: $CuCl_{2(aq)} \rightarrow CuCl_{2(s)}$. Crystallization's main advantage is the relatively low energy requirements compared to other drying techniques such as spray-drying. Experiments have shown that precipitation and dissolution occur at different temperatures [36]. Crystals begin to form at colder temperatures and dissolve at lower temperatures than predicted by a simple solubility model. The difference between these two temperatures is the metastable zone width (MSZW = T_d – T_{met}). Thus, metastability delays phase change compared to a simple solubility model prediction and the dissolution and precipitation temperatures dependent on the direction, as well as rate of temperature change.

As illustrated by Figure 4.1, metastability is a type of chemical hysteresis and a critical parameter for optimal design of a crystallization system. The main importance of metastability to the Cu-Cl cycle is that precipitation (e.g., crystallization) occurs at a lower temperature (T_{met}) and thus reduces thermal energy requirements.

Another important factor for effective design of crystallization equipment is the solubility equilibrium, which is described by the solubility product constant, K_{sp}. The dimensionless parameter K_{sp} indicates the extent of solubility of a substance in a water

solvent. The solubility product constant is a logarithmic scale, and higher K_{sp} indicates higher solubility. The solubility product constant for soluble chemicals is typically on the order of approximately 10^{-5}, however, K_{sp} for $CuCl_2$ (which dissolves readily in water), is several orders of magnitude higher, at approximately 1. Euler, Kirschenbaum and Ruekberg [37] provide equations for calculating K_{sp} in terms of G (Gibbs free energy), and equations for calculating G in terms of H (enthalpy), T (temperature), and S (entropy). The variable K_{sp} is usually calculated in terms of concentration, but the equations given in Euler, Kirschenbaum and Ruekberg [37] are essential for calculating K_{sp} as a function of temperature.

The objectives of the metastability experiments are to investigate the relationship between cooling rate and MSZW for $CuCl_2$-H_2O-HCl (ternary) systems, as well as to determine K_{sp} values for $CuCl_2$ dissolving in H_2O-HCl systems. The values of K_{sp} have not previously been determined for $CuCl_2$ dissolving in H_2O-HCl systems.

4.2.1 Metastability Experimental Method

MSZW is determined by cooling an unsaturated solution until a crystal appears, and then gradually heating the solution until the crystal re-dissolves. MSZW is the difference between the temperatures of appearance (T_{met}) and disappearance (T_d). An HCl solution of known molarity is prepared in a jacket vessel by diluting an 12M $HCl_{(aq)}$ with a corresponding volume of water to make 200 mL of solution. The specified amount of $CuCl_2$ is weighed and added to the jacket vessel. The solution is continuously stirred at 300 to 350 RPM with a magnetic stirrer. A programmable heater/chiller that circulates ethylene-glycol solution through the jacket vessel controls the solution temperature, as well as the heating/cooling rates. The temperature of the solution is measured with a digital thermocouple.

As shown by Figure 4.1, the solution is heated to $T_{initial}$, and held there until all $CuCl_2$ is dissolved (resulting in a homogenous mixture). Next, the solution is cooled at a constant rate (dT/dt) until the first crystal appears at T_{met}. The solution is then heated at a constant rate, until the crystal re-dissolves at T_d. The magnitude of cooling and heating rates may be different. K_{sp} is determined by calculations made from the MSZW experimental data and reference data.

4.2.2 Formulation of Metastability & Equilibrium

The most general form of the equation relating cooling rate to MSZW is given in Equation 4.2 from [36]:

$$\ln\left(\frac{dT}{dt}\right) = m\ (\text{MSZW}) + \ln(k_N) + (m-1)\ln\left(\frac{dc^*}{dT}\right) - \ln(\epsilon) \tag{4.2}$$

where ϵ is a conversion factor given by Equation 4.3.

$$\epsilon = \frac{100\, R_{ha}}{(100 - c_N(R_{ha} - 1))^2} \tag{4.3}$$

R_{ha} is ratio of the molecular weight of the hydrated form of a compound to that of the anhydrous from of the same compound [36]. A hydrate of $CuCl_2$ is $CuCl_2{\cdot}2H_2O$. R_{ha} for $CuCl_2$ is calculated as:

$$R_{ha} = \frac{MM_{CuCl_2 \cdot 2H_2O}}{MM_{CuCl_2}} = \frac{134.45\ g/mol + 2 \times 18.02\ g/mol}{134.45\ g/mol} = 1.268 \tag{4.4}$$

According to Barrett and Glennon [36], for a plot of $\ln(\frac{dT}{dt})$ vs. ln(MSZW); the slope is equal to the nucleation order, m_N, and the y-intercept is equal to $\ln(k_N)$, where k_N is the nucleation order, $k_N = e^{y-intercept} = e^{\ln(k_N)}$.

$$\ln\left(\frac{dT}{dt}\right) = m\ \ln(MSZW) + \ln(k_N) \tag{4.5}$$

The exact version of Equation 4.5 proposed by Barrett and Glennon [36] is an empirical correlation (from potash alum data), which has of $m_N = 2.03$ and $\ln(k_N) =$ -8.967, the values of which vary depending on the chemicals in the solution.

The solubility equilibrium is determined in the following way. The variable K_{sp} is calculated by first calculating the difference in Gibbs Free Energy at the reference state (ΔG°), from Equations 4.6 and 4.7.

$$\Delta G^\circ = -RT\ \ln(K_{sp}) \tag{4.6}$$

$$\Delta G^\circ = \Delta H^\circ - T\Delta S^\circ \tag{4.7}$$

ΔH° and ΔS° of the solution are calculated as weighted-averages from thermophysical data by Equations 4.8 and 4.9 with component masses as the weight factors.

$$\Delta H^\circ = m_{HCl}\, H_{HCl} \times (1 - m_{HCl})\, H_{water} \tag{4.8}$$

$$\Delta S^\circ = m_{HCl}\, S_{HCl} \times (1 - m_{HCl})\, S_{water} \tag{4.9}$$

4.2.3 Metastability Results and Discussion

As presented in Table 4.1, to determine the unknown variables in Equation 4.5 and to ensure independence from concentration, average and weighted-average values for m_N (slope), and $\ln(k_N)$ (y-intercept) are calculated. The calculation uses the number of data points per concentration divided by the total number of data points as the weights.

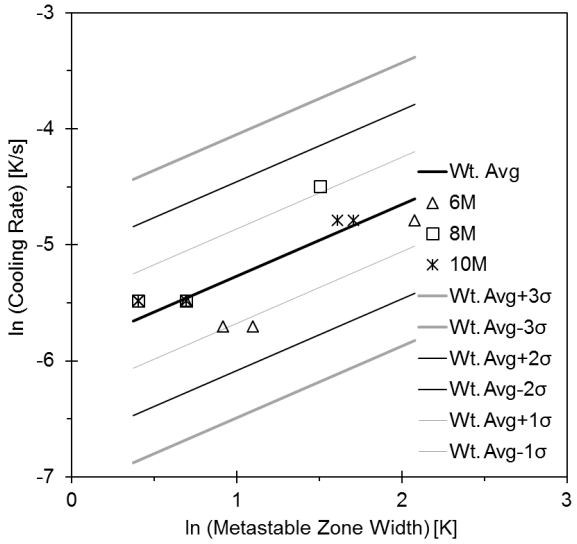

Figure 4.2: Experimental Data on Metastable Zone Width of $CuCl_2$ in H_2O.

Table 4.1: Nucleation Order and Nucleation Rate Constants for Several HCl Concentrations.

HCl Conc. [mol/L]	**m_N (Slope) [-]**	**$\ln(k_N)$ (y-Intercept) [-]**	**k_N [-]**	**Number of Data Points**
6	0.621	-6.162	2.107×10^{-3}	4
8	0.998	-6.056	2.343×10^{-3}	4
10	0.362	-5.592	3.728×10^{-3}	5
Mean	0.660	-5.937	2.640×10^{-3}	
Wt.Avg	0.637	-5.910	2.711×10^{-3}	

As presented in Figure 4.2, the nucleation order and nucleation rate constants are almost all within 1 σ of the weighted average (Wt. Avg). Cooling rate has a dominant influence on MSZW, whereas concentration has a minor influence on MSZW. It is likely that HCl acts as a crystallization inhibitor, since MSZW is found to decrease slightly with HCl concentration, as shown by Figure 4.3.

The relation between MSZW and HCl concentration is plotted in Figure 4.3, for various cooling rates. Linear fits are applied for 0.25 K/s and 0.5 K/s. For the 0.5 K/s dataset, the point at (4,5) is probably an outlier, thus two linear fits are applied; one including the outlier and the other without. The linear fit without the outlier has a stronger linear correlation. Further experimentation is required to determine if the point at (4,5) is an outlier.

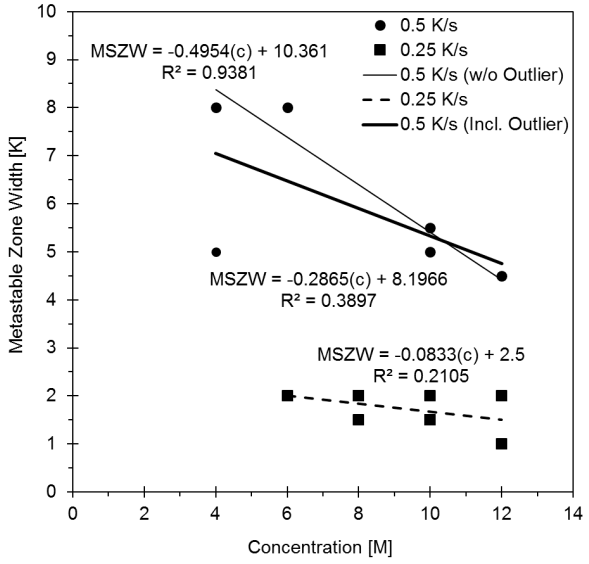

Figure 4.3: Effect of Cooling Rate on Metastable Zone Width for $CuCl_2$ in H_2O.

As illustrated by Figure 4.3, MSZW decreases with concentration and MSZW increases with cooling rates, which agrees well with previous experimental results [38]. This is likely caused by higher cooling rates, producing a lower temperature before observing the first crystal, thus lowering T_{met} and increasing MSZW. If the temperature is decreasing too rapidly, T_{met} may be passed because the solution was unable to crystallize at the maximum value of T_{met} due to the rapid cooling rate. When the cooling rate is slower, the solution has time to begin crystallizing at the maximum value of T_{met}.

A higher nucleation order (m_N) means that the nucleation mode of crystallization (creating new crystals, thus increasing the integer count of crystals), dominates over the growth mode of crystallization (increasing the average size of crystals). As presented in Table 4.2, values of m_N and y-intercept are determined for a ternary system, and a correlation is not apparent between the concentration of HCl and the nucleation order.

Table 4.2: Nucleation Order and Rate for $CuCl_2$ in H_2O-HCl.

HCl Conc. [mol/L]	**m_N (Slope) [-]**	**$\ln(k_N)$ (y-Intercept) [-]**
2	n/a	n/a
4	0	-4.787
6	0.621	-6.162
8	0.998	-6.056
10	0.362	-5.592
12	0.472	-5.595

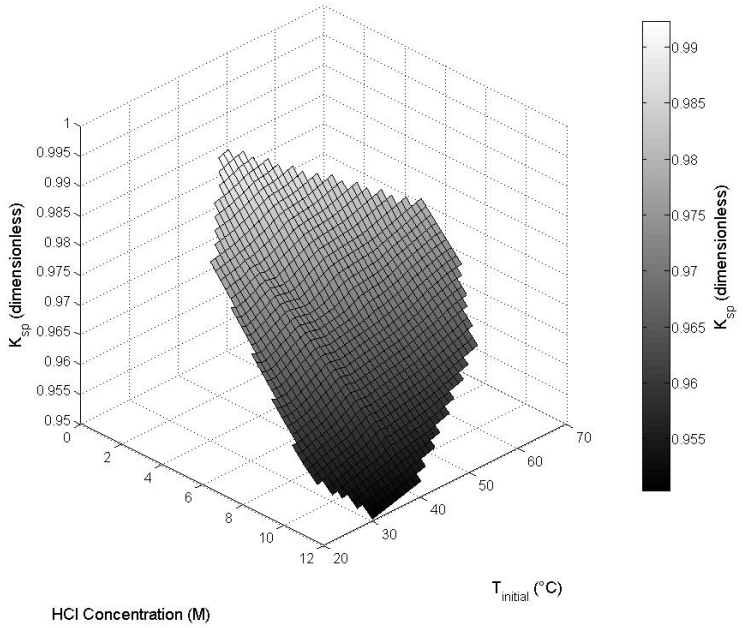

Figure 4.4: Solubility of $CuCl_2$ Dissolving in HCl Solutions of Different Molarities.

As illustrated in Figure 4.4, the relation between HCl concentration, $T_{initial}$ and K_{sp} is investigated for a ternary systems. The effect of $CuCl_2$ is neglected because it is not a fluid. Linear extrapolation is performed for hydrogen chloride data when $T \geq 60$℃. The pressure is assumed to be 100 kPa for thermophysical data. The variable K_{sp} increases with temperature, since at higher temperatures there is more Brownian motion and more molecular interaction, and hence the solubility increases. The variable K_{sp} also decreases with HCl concentration, because HCl acts as an anti-solvent, reducing the solubility of $CuCl_2$ in higher concentrations of HCl solution. The surface can be modelled by Equation 4.10.

$$\begin{gathered} K_{sp} = 0.9968 - 0.005882(c_{HCl}) + 0.0001015(T_{initial}) + \\ 0.000131(c_{HCl})^2 + 2.776 \times 10^{-6}(c_{HCl})(T_{initial}) + 1.393 \times 10^{6}(T_{initial})^2 \end{gathered} \tag{4.10}$$

4.2.4 Metastability Conclusions

There is found to be a substantial positive correlation between cooling rate and MSZW. If the crystallization process is not gradual, it is likely maximum T_{met} will be surpassed (reducing T_{met} and increasing MSZW). The presence of a MSZW decreases the precipitation (i.e., crystallization) temperature, resulting in thermal energy savings.

The apparent dependency of MSZW on HCl concentration, as shown in Figure 4.3, is slightly detrimental to the Cu-Cl cycle, because it is preferred that MSZW be as wide as possible and that it also be independent of HCl concentration. In that manner, the precipitation temperature, T_{met}, would be as low as possible, thus reducing the energy requirements of crystallization.

The results on MSZW should be treated as only tentative, due to significant noise. Further experimentation (ideally with more sophisticated nucleation detection methods) is required to identify the cause of the noise and to overcome the noise.

For solubility equilibrium, K_{sp} increased with temperature (as expected) and decreased with HCl concentration (the effect of HCl concentration on K_{sp} was previously unknown). The metastability results provide useful new experimental data for crystallization and metastability in the Cu-Cl cycle.

Chapter 5

Distillation Simulation

5.1 Thermodynamic Models

Chemical simulation software requires the user to select a thermodynamic model which predicts how the chemical system behaves (i.e., the thermochemical and thermophysical properties) under varying conditions (e.g., bubble point temperature varying with respect the concentration of one component of a binary mixture). The user must select a suitable model; an unsuitable model causes inaccurate results. A "wizard" within the software and/or an external flowchart may assist the user with model selection.

Thermodynamic models are used for many purposes, including:

- generating phase diagrams (Figure 5.2) and x-y (VLE) plots
- property calculations (e.g., enthalpy of a phase, of a component (chemical species), or entire mixture, at a known temperature and pressure)
- simulating process flows

Simulations are performed using CAPE (Computer-Aided Process Engineering) software. CAPE-OPEN is a standard for CAPE. Initially, COCO (CAPE-OPEN to CAPE-OPEN) simulation software is used. The UNIQUAC (Universal Quasi-Chemical) model is used within COCO. It is selected because it is the only model supported in COCO which shows azeotropes when plotting HCl-water phase diagrams. Other models supported by COCO (e.g., Peng-Robinson) are unsuitable for HCl-water as they result in phase diagrams without azeotropes. However, the UNIQUAC model has limitations when plotting HCl-water phase diagrams. For example, as shown in Figure 5.1, the dew point (upper) curve is discontinuous at its left when plotted at a pressure of 1 bar.

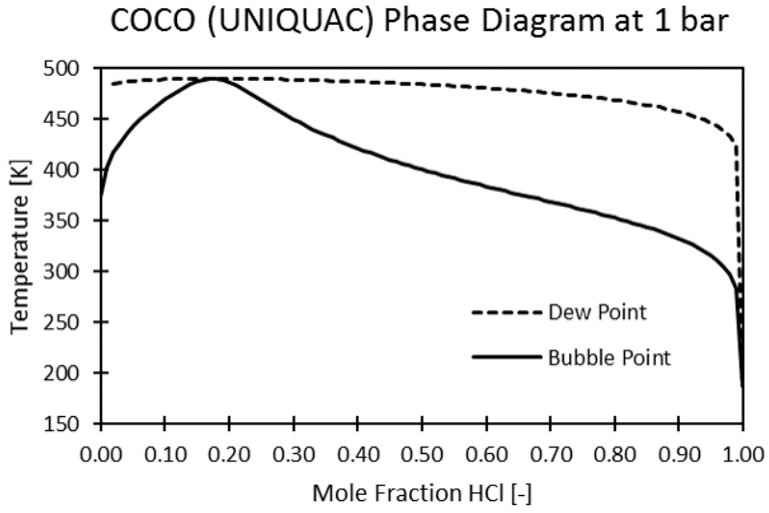

Figure 5.1: Phase diagram at 1 bar, data generated in COCO using the UNIQUAC model. Note the discontinuity on the dew point (upper) curve.

5.2 Simulation Setup

Chemcad, another CAPE software, is used to generate phase diagrams and simulate a pressure-swing distillation system. The PPAQ (Partial Pressure of Aqueous Solutions) model, an electrolyte model, is used to calculate the K-value ($K_i = y_i/x_i$). The SRK (Soave-Redlich-Kwong) model used to calculate the H-value (enthalpy). These models are suggested by Chemcad's "wizard" based on the user's choices of components (in this case, HCl and H_2O). A flowchart, such as those in [39] or [40], can also assist with model selection.

Chemcad is also used to plot phase diagrams. Phase diagram data (in tabulated form) is generated in Chemcad using the PPAQ model. As shown by Figure 5.2, the azeotropic concentration decreases slightly with pressure.

A process flow diagram of PSD with heat integration is created in Chemcad, as shown in Figure 5.3. The streams (e.g., feed, distillate) and unit operations (e.g., pump, distillation column) are taken from the palette and placed in the process flow diagram via drag-and-drop. The user then selects each stream and unit operation and sets its properties (e.g., temperature, pressure, number of stages). Fundamentally, Chemcad iteratively solves a system of equations. Entering properties constrains the simulation, by making the degrees of freedom of the system of equations equal to zero. For the simulation to be solvable, the number of unknowns must be equal to the number of equations. Initial guesses of the unknown variables (column top and bottom temperatures) are estimated by

the software or can be entered by the user. The system of equations is solved iteratively until the solution converges within a certain tolerance (1×10^5 for flash calculations, 0.001 for other parameters) or until a certain number of iterations (default or user-set) are performed. The converge tolerance and maximum number of iterations can be changed by the user.

The low-pressure column (item 1 in Figure 5.3) is set to 1 atm and the high-pressure column (item 3 in Figure 5.3) is set to 10 atm. Using trial-and-error, it is determined that the ideal number of stages is 7 per column (too few stages results in an insufficient degree of separation). It is also determined that the feed stage should be stage 6 (where stage 1 is at the top). Certain parameters such as the heat exchanger duty, must be assumed. It is set to 500 W. The properties of the input stream (stream 1) are specified by the user and given in Table 5.1. The process flow diagram of Figure 5.3 is solved and the results are shown in Tables 5.1 to 5.5.

5.3 Simulation Results

5.3.1 Pressure-Swing Distillation

The compositions of the streams shown in Figure 5.3 are given in Table 5.1. Please note that Checmad software gives results with a large number of significant figures, more than can be expected of a physical experiment. Such a high degree of accuracy is not applicable outside the simulation.

Table 5.1: Simulation Results: Stream Compositions

Stream No.	1	2	3	4
Temperature [K]	**298.0***	379.1	380.1	380.4
Pressure [atm]	1.000*	0.999	0.999	10
Enthalpy Rate [J/s]	-2.676×10^5	-1.84×10^5	-77,870	-77,870
Vapor mole frac. [-]	0	0	0	0
Total flowrate [mol/s]	1	0.699	0.301	0.301
Total flowrate [g/s]	19.860	13.802	6.058	6.058
Total std liquid flowrate [m^3/h]	0.0739	0.0512	0.0226	0.0226
Total std vapour flowrate [m^3/h]	80.69	56.4	24.29	24.29
HCl flowrate [g/s]	3.646	2.390	1.2560	1.2560
H_2O flowrate [g/s]	16.21	11.41	4.802	4.802
Stream No.	5	6	7	8

Temperature [K]	242.1	**449.3**	**304.6***	**428.0**
Pressure [atm]	10	10	0.9990*	9.999
Enthalpy Rate [J/s]	-108.7	-76,170	-2.670×10^5	-76,670
Vapor mole frac. [-]	0	0	0	0
Total flowrate [mol/s]	0.001	0.3	1	0.3
Total flowrate [g/s]	0.0363	6.022	19.86	6.022
Total std liquid flowrate [m^3/h]	0.0002	0.0225	0.0739	0.0225
Total std vapour flowrate [m^3/h]	0.08	24.21	80.69	24.21
HCl flowrate [g/s]	0.0362	1.220	3.646	1.220
H_2O flowrate [g/s]	0.0001	4.802	16.21	4.802

As shown in Table 5.1, the feed stream (stream 1) contains a mixture of HCl and H_2O; ($\dot{m}_{HCl}$ = 3.65 g/s, $\dot{m}_{H_2O}$ = 16.21 g/s). The LPC distillate (stream 2) is primarily H_2O; ($\dot{m}_{HCl}$ = 2.39 g/s, $\dot{m}_{H_2O}$ = 11.41 g/s). The HPC distillate (stream 5) is almost pure HCl; ($\dot{m}_{HCl}$ = 0.04 g/s, $\dot{m}_{H_2O}$ = 0.0001 g/s). So, by mass: the LPC distillate is 82.7 % H_2O, and the HPC distillate is 99.8 % HCl. Thus, the simulated system separates H_2O from HCl with limited effectiveness (in the LPC), but separates HCl from H_2O very effectively (in the HPC).

Distillation profiles (temperature, pressure and flowrates for each plate (stage)) for the LPC and HPC are given in Tables 5.2 and 5.3, respectively. The flowrates for stages 2-6 are blank, as these stages are intermediary stages, meaning they are neither feed (input) nor product (output). The heat duty is also blank as they are not connected to the condenser or reboiler.

Table 5.2: Simulation Results: LPC Distillation Profile

Stage	Temp [K]	Pressure [atm]	Liquid flowrate [g/s]	Vapor flowrate [g/s]	Feed flowrate [g/s]	Product flowrate [g/s]	Heat Duties [J/s]
1	379.1	1.00	102.62			13.80	-2.213×10^5
2	380.1	1.00	105.93	116.42			
3	380.1	1.00	106.52	119.73			
4	380.1	1.00	106.62	120.32			
5	380.1	1.00	106.64	120.42			
6	380.1	1.00	130.12	120.44	19.86		
7	380.1	1.00		124.07		6.06	2.27×10^5
Mass Reflux Ratio					7.435		
Total liquid entering stage 6 at 368.2 K [g/s]					126.5		

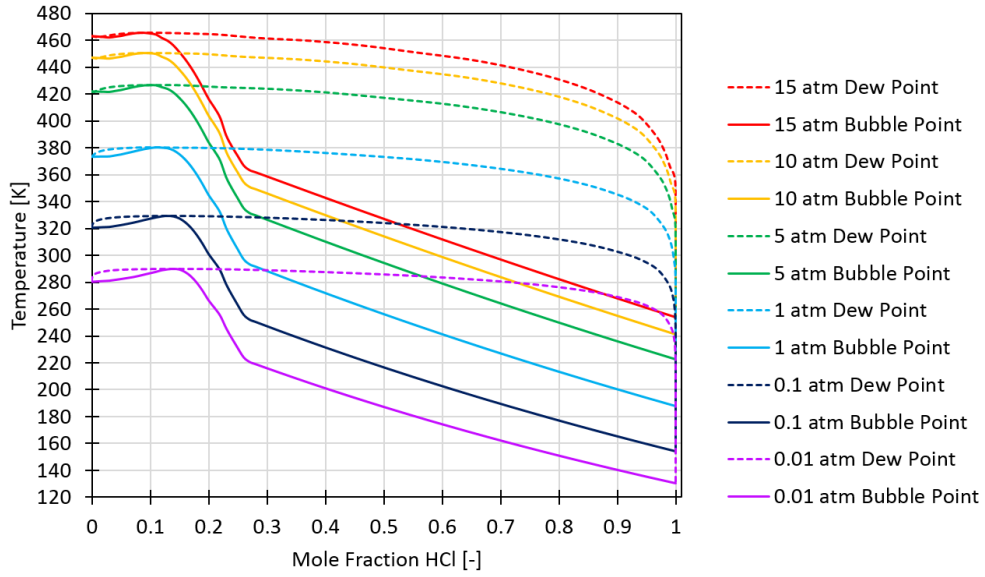

Figure 5.2: Phase diagram generated in Chemcad using the PPAQ model.

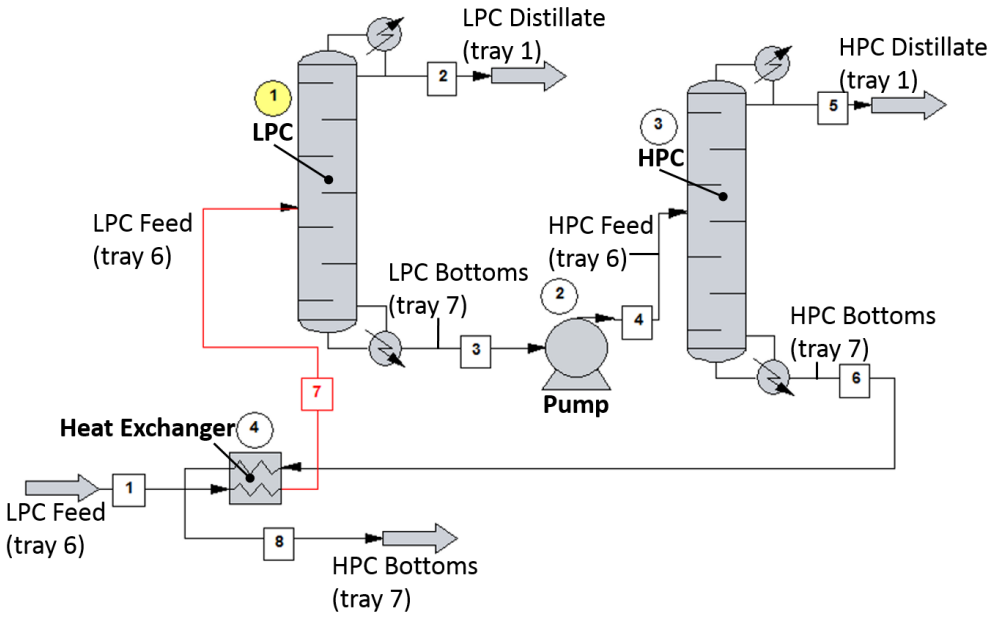

Figure 5.3: Chemcad process flow diagram of pressure-swing distillation with heat integration.

Table 5.3: Simulation Results: HPC Distillation Profile

Stage	Temp [K]	Pressure [atm]	Liquid flowrate [g/s]	Vapor flowrate [g/s]	Feed flowrate [g/s]	Product flowrate [g/s]	Heat Duties [J/s]
1	242.1	10.00	0.27			0.04	-142.5
2	350.4	10.00	0.08	0.30			
3	442.9	10.00	0.08	0.12			
4	446.3	10.00	0.08	0.11			
5	446.5	10.00	0.08	0.11			
6	446.5	10.00	7.22	0.11	6.06		
7	449.3	10.00		1.20		6.02	1731
Mass Reflux Ratio					7.357		
Total liquid entering stage 6 at 381.2 K [g/s]					6.134		

The simulated LPC (Table 5.2) and HPC (Table 5.3), are found to have reflux ratios of 7.44 and 7.36, respectively. Reflux ratio is the ratio of the amount product re-entering the column over the amount of product leaving the top of the column as distillate. The use of reflux is not mandatory, however a higher reflux ratio tends to result in a higher purity of the distillate, as it passes through the column several times before finally leaving. In the interest of simplicity, the actual column is not intended to have any reflux (zero reflux ratio). However, due to the modularity of piping components, a reflux loop can be added at a later time.

The LPC and HPC tray compositions are given in Tables 5.4 and 5.5, respectively, which show the mass flowrates of the components (HCl, H_2O) and phases (vapour, liquid) at each tray (stage). The concentration (as a mass fraction) can be computed from the mass flow rates. The data tabulated in Tables 5.4 and 5.5 is plotted in Figure 5.4.

Table 5.4: Simulation Results: LPC Tray Composition Data

Stage 1	379.12 K	1.00 atm	
	$\dot{m}_{Vapor}$ [g/s]	$\dot{m}_{Liquid}$ [g/s]	K [-]
HCl	0.0000	17.77	0.0000
H_2O	0.0000	84.85	0.0000
Total [g/s]	0.0000	102.6	
Stage 2	380.10 K	1.00 atm	
HCl	20.16	21.24	0.8506
H_2O	96.26	84.69	1.019
Total [g/s]	116.4	105.9	
Stage 3	380.10 K	1.00 atm	

HCl	23.63	21.89	0.9558
H_2O	96.10	84.62	1.006
Total [g/s]	119.7	106.5	
Stage 4	380.10 K	1.00 atm	
HCl	24.28	22.01	0.9752
H_2O	96.04	84.61	1.003
Total [g/s]	120.3	106.6	
Stage 5	380.09 K	1.00 atm	
HCl	24.40	22.03	0.9786
H_2O	96.02	84.61	1.003
Total [g/s]	120.4	106.6	
Stage 6 (Feed)	380.09 K	1.00 atm	
HCl	24.42	26.88	0.9792
H_2O	96.02	103.2	1.003
Total [g/s]	120.4	130.1	
Stage 7	380.09 K	1.00 atm	
HCl	25.63	1.256	0.9958
H_2O	98.44	4.802	1.000
Total [g/s]	124.1	6.058	

Table 5.5: Simulation Results: HPC Tray Composition Data

Stage 1	242.06 K	10.00 atm	
	$\dot{m}_{Vapor}$ [g/s]	$\dot{m}_{Liquid}$ [g/s]	K [-]
HCl	0.0000	0.2661	0.0000
H_2O	0.0000	0.0007	0.0000
Total [g/s]	0.0000	0.2667	
Stage 2	350.40 K	10.00 atm	
HCl	0.3022	0.0348	3.643
H_2O	0.0008	0.0458	0.00690
Total [g/s]	0.3030	0.0806	
Stage 3	442.93 K	10.00 atm	
HCl	0.0710	0.0192	3.117
H_2O	0.0459	0.0587	0.6583
Total [g/s]	0.1169	0.0778	
Stage 4	446.32 K	10.00 atm	
HCl	0.0553	0.0174	2.5067
H_2O	0.0588	0.0592	0.7814
Total [g/s]	0.1141	0.0766	

Stage 5	446.47 K	10.00 atm	
HCl	0.0536	0.0172	2.454
H_2O	0.0593	0.0593	0.7910
Total [g/s]	0.1129	0.0765	
Stage 6 (Feed)	446.48 K	10.00 atm	
HCl	0.0534	1.626	2.450
H_2O	0.0594	5.593	0.7917
Total [g/s]	0.1128	7.219	
Stage 7	449.35 K	10.00 atm	
HCl	0.4067	1.220	1.817
H_2O	0.7910	4.802	0.8975
Total [g/s]	1.198	6.022	

As shown by Figure 5.4, the LPC distillate has a mass fraction of HCl of 0.173, whereas the HPC distillate has a mass fraction of HCl of 0.998. The horizontal asymptote for the LPC curves is the azeotropic concentration at 1 atm (approximately 0.11 mass fraction HCl). The horizontal asymptote for the HPC curves is the azeotropic concentration at 10 atm (approximately 0.09 mass fraction HCl). Although it may appear otherwise, the two sets of curves do not actually converge. If one closely observes the curves of Figure 5.4 at tray 7, it is evident that the HPC liquid curve is below both LPC curves. As shown by Figure 5.3, the LPC bottoms (LPC tray 7) is pressurized from 1 atm to 10 atm and enters the HPC as feed (HPC tray 6). However, the quality decreases due to the pressure rise.

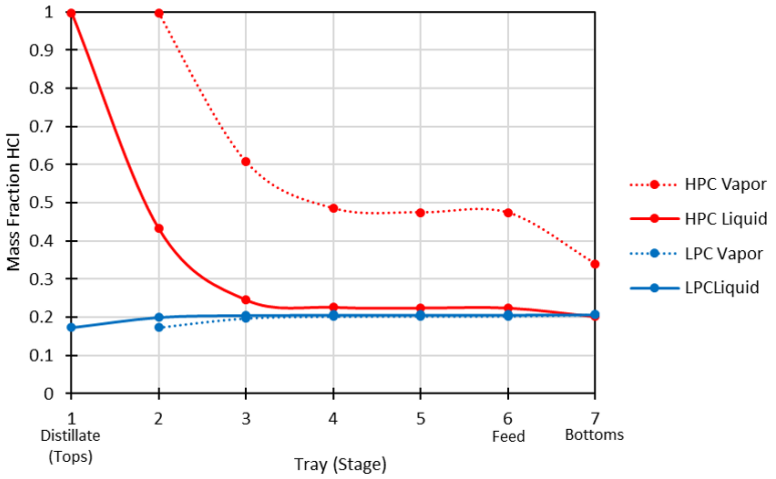

Figure 5.4: Simulation Results: Tray Compositions.

5.3.2 Single-Column Distillation

A simulation is also performed for single-column distillation, as shown in Figure 5.5. Results are given in Table 5.6.

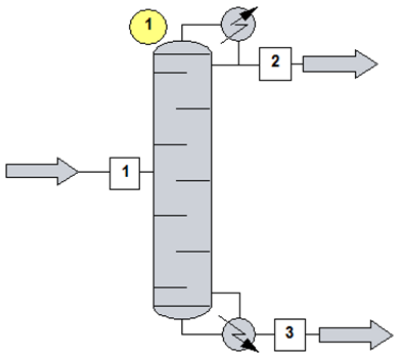

Figure 5.5: Chemcad process flow diagram of single column distillation.

Table 5.6: Single-Column Simulation Results

Identifier	$\mathbf{x_{feed}}$ **[mol/mol]**	$\mathbf{x_{output}}$ **[mol/mol]**
1D	0.01	0.00
1B	0.01	0.03
2D	0.03	0.00
2B	0.03	0.10
3D	0.05	0.03
3B	0.05	0.11
In the 1st column, D and B signify distillate and bottoms, respectively.		

The results of the single-column distillation simulation are such that:

$$\begin{gathered} 0 \leq x_{\text{distillate}} \leq x_{\text{feed}} \leq x_{\text{bottoms}} \leq x_{\text{azeotropic}} \\ \text{where } x_{\text{azeotropic}} = 0.11 \text{ mol/mol} \end{gathered} \tag{5.1}$$

The results shown in Table 5.6 satisfy the criteria of Equation 5.1. All concentrations are less than or equal to azeotropic, which is reasonable since it is impossible to cross the azeotrope with one column operating at a constant pressure.

5.4 Simulation Conclusion

The results in Table 5.1, while encouraging, should be interpreted cautiously, as there are substantial differences between the simulated columns and the actual column. For example, the simulated columns are perforated-plate (tray) columns, where as the actual column is a packed column. Also, as shown in Table 5.3, stage 1 of the HPC is found to be

242.1 K (-31.05 ℃), which is unfeasible, since active cooling would be required to achieve such a temperature. Furthermore, the simulated distillation is run in continuous mode (constant mass/molar flow rates in/out at steady state), whereas the actual distillation is run in batch mode. The use of continuous mode in simulation explains the fairly high mass flow rates found in the simulation (e.g., in Table 5.1; $\dot{m}_1 = 19.8596$ g/s). Consequently, the high mass flow rates explain the high heat duty of the LPC reboiler (2.27×10^5 J/s (stage 7 in Table 5.2)). In the actual distillation, the batch size is $<$ 100 g, therefore the heat duties (heat inputs) are expected to be significantly less than those found via simulation. Batch mode is used in the actual distillation as it eliminates the feed pump (an expensive device which must be protected against corrosion). A feed pump is not required in batch mode, as a batch of feed can enter the column from a feed chamber via gravity. The simulated PSD system includes heat integration, however, to decrease construction cost, the actual system is not intended to comprise heat integration, although it could be added at a later time.

The simulation predicts a large degree of separation and its results could possibly be used as a benchmark against which to compare experimental results.

Chapter 6

Apparatus Design

One column is adequate for validation because it can produce pure HCl (but not pure water). However, HCl is more valuable than water, for the purpose of the Cu-Cl cycle. If concentration of the feed is greater than the azeotropic concentration, it is possible to achieve pure HCl, but not pure H_2O, as pure H_2O lies on the opposite side of the azeotrope (as shown in Figure 5.2). Therefore, even by only extracting pure HCl, the efficiency of the Cu-Cl cycle is still increased. Obtaining pure HCl is an important step toward integration of the Cu-Cl cycle.

Crossing the azeotrope (for a binary mixture) using only one pressure, requires the use of a 3^{rd} component (the entrainer), into which one of the mixture's initial components dissolves. After the two initial components are separated from each other, the entrainer must then be separated from one of the initial components. This process is collectively known as extractive distillation.

Distillation requires surfaces (i.e., stages) on which VLE can occur (i.e., the rates of evapouration and condensation are equal). Usually, these stages are perforated plates, which allow vapour to rise upward through the small perforations in the plates, but prevent liquid from falling through the perforations due to surface tension. Since the components have different boiling temperatures, and each stage is held at a different temperature, the concentration (e.g., mole fraction of component i) of the vapour and liquid phase are different at each stage. In this way, separation is achieved.

Structured or random packings (e.g., Raschig rings) can also be used as VLE surfaces. The length of packed column which achieves the same amount of separation as a theoretical plate is referred to as the height equivalent to a theoretical plate (HETP).

6.1 Column Pressure

The vapours rise in the column due to a pressure gradient from the bottom of the column to the top, as well as by buoyancy (i.e., density gradient). A heat flux is applied to the column such that the bottom of the column is hotter than the top. Therefore, the vapours at the bottom of the column have higher temperature, higher pressure and lower density than those at the top, so they rise. Liquid in the column falls due to gravity.

During normal operation, the maximum pressure at any location in the column should only be slightly greater than atmospheric (101.325 kPa). This slight pressure rise is caused by the temperature increase of the solution vapours as the column is heated. Pressure increases may also be caused by the column packing, which acts as a flow restrictor, allowing slight pressure gradients to develop instead of allowing the pressure to equalize along the height of the column (as would occur in an unobstructed column). The column includes a pressure relief valve rated for 861 kPa (125 psi). The pressure relief valve rating of 125 psi is less than the rating of the weakest components (iron pipe fittings rated for 150 psi). Therefore, $HCl_{(g)}$ and $H_2O_{(g)}$ vapour is vented, before the pressure could increase sufficiently to rupture the column.

6.2 Experimental Setup Components

The column is packed with ceramic Raschig rings, which are in the shape of hollow cylinders with OD = 6.1 mm, ID = 2.5 mm, and height = 5.5 mm. These Raschig rings have a surface-area-to-volume ratio, ω, of approximately 2135 m^2/m^3. At any one point among the Raschig rings, the rates of evapouration and condensation are equal, although these rates vary from point to point. A fractional voidage (volume occupied by packing/total column volume), ϵ, of 0.8 m^3/m^3 is assumed. The PVC hoses, which connect the top (distillate product) and bottom (bottoms product) of the column to their respective output chambers, act as condensers or heat exchangers with the ambient air in order to remove heat from the distillate and bottoms products.

The materials of the components which comprise the output chambers are given in Figure 6.1.

Qualitative corrosion resistance data from [41] is examined for several metals as shown in Table 6.1. Hasteloy B exhibits the best corrosion resistance, however, its cost is approximatively 7 times that of stainless steel. Thus, 316 stainless steel is chosen, despite suboptimal corrosion resistance, as it can be used for multiple runs before corroding to the point of unusability (42,000 mpy in 50% HCl at 230 F [42]), (mpy = mils per year, 1 mil = 1/1000 inch). The column is built with NPT pipe, because it is ubiquitous and modular.

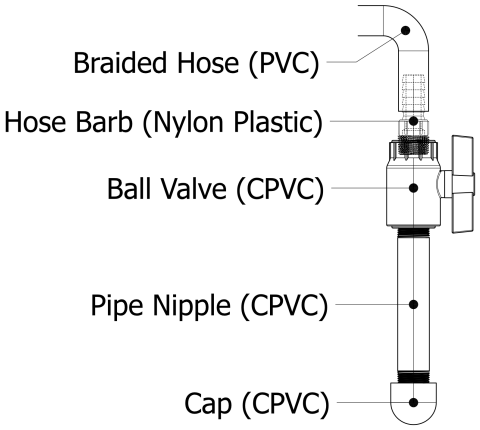

Figure 6.1: Output Chamber Detail.

Table 6.1: Corrosion Resistance, Data from [41].

1) Good, 2) Be Careful, 3) Not Useable		
Material	**$HCl_{(aq)}$, aerated**	**$HCl_{(aq)}$, air free**
316 Stainless Steel	3	3
416 Stainless Steel	3	3
Cast Iron	3	3
Carbon Steel	3	3
Hasteloy B	1	1
Hasteloy C	2	2
Titanium	1/2	1/2

6.2.1 Estimation of Mass Loss due to Corrosion

The mass lost due to corrosion, m_{lost} in mg, over a time period, $t_{exposure}$, can be estimated using Equation 6.1 [43].

$$m_{lost} = \frac{\dot{L}}{87.6} \cdot \rho_{metal} \cdot A \cdot t_{exposure} \tag{6.1}$$

Where $\dot{L}$ is the corrosion rate in mm/year, ρ_{metal} is the metal density in g/cm^3, A is the exposed in area in cm^2 and $t_{exposure}$ is the exposure time in hours.

The exposed area, A in cm^2, can be expressed as the surface area of a cylinder:

$$A = \pi(ID)\, z \tag{6.2}$$

where ID is the column internal diameter in cm, and z is the column height in cm.

Table 6.2: Parameters for Calculating m_{lost}.

Quantity	**Value**	**Comment**
m_{lost} [mg]	163338	Computed via Equation 6.1.
m_{lost} [g]	163.34	
m_{lost} [%]	5.597	Mass lost as percent of $m_{pipe,\ initial}$.
$\dot{L}$ [mm/year]	1066.8	Value from [42], converted from mpy.
OD [cm]	2.667	From [44], assuming standard pipe schedule.
ID [cm]	2.093	Computed from OD and wall thickness from [44], assuming standard pipe schedule.
z [cm]	170.2	Computed via Equation 7.2.
A [cm^2]	1119.104	Computed via Equation 6.2.
ρ_{metal} [g/cm^3]	7.99	From [45].
$t_{exposure}$ [h]	1.5	Assumed based on typical experiment time.
$m_{pipe,\ initial}$ [g]	2918.4	Computed via Equation 6.3.

The mass of the pipe (i.e., column), m_{pipe} in g, can be expressed as:

$$m_{pipe} = \rho_{metal} \cdot \frac{\pi}{4} \cdot z \cdot (OD^2 - ID^2) \tag{6.3}$$

where OD is the column external diameter in cm.

Results of the computation of Equations 6.1 to 6.3 are given in Table 6.2.

The computation of Equations 6.1 to 6.3 predicts that the column loses approximately 5.6% of its mass per experiment. However, this figure is a conservative estimate. The actual mass loss may be substantially lower for several reasons. Namely, HCl is usually in contact with column material for substantially less than $t_{exposure}$. Furthermore, the corrosion exposure area, A, is usually less than that given in Table 6.2, because HCl does not make uniform contact with the column. Instead, it makes non-uniform or irregular contact, that is, some areas of the column contact HCl whereas as others do not, due to the stochastic component(s) of fluid movement in the column (e.g., that caused by turbulence).

6.3 Output Analysis

The usable interior volume of each output chamber, v_{empty}, was determined by filling each chamber with water and measuring the volume of the water when it is poured out into a graduated cylinder. The pressure in each output chamber, P_{gage}, was measured with a mechanical gage and the temperature was measured with a mechanical temperature gage.

Before the distillation begins, the mass of each empty output chamber, m_{empty}, was measured. Once the distillation is complete, the exterior of each chamber was wiped and dried to remove any external fluid which would cause the measurements to be overestimated. The mass of the chamber, m_{full}, was measured. Then each output chamber valve is opened briefly, allowing the vapour phase to escape. The valves are closed and the mass of the chamber without the vapour phase, (m_{full} - m_g), was measured. Then the liquid phase in each chamber is poured into a graduated cylinder and v_l is measured. The mass of the chamber without both phases, (m_{full} - m_g - m_l), was also measured; it should be approximately equal to m_{empty}, since once the vapour and liquid phases are removed, there should be nothing more in the chamber. To minimize random error (noise), each mass value reported is the average of three measurements. Repeated measurements are not performed for volume because a small amount of liquid remains in the graduated cylinder after each pour which would cause a systematic error.

The mass of the vapour phase, m_g, and the mass of the liquid phase, m_l, are calculated by Equations 6.4 and 6.5, respectively.

$$m_g = m_{full} - (m_{full} - m_g) \tag{6.4}$$

$$m_l = (m_{full} - m_g) - (m_{full} - m_g - m_l) \tag{6.5}$$

The volume of the liquid phase, v_l, was measured by pouring the contents of the output chamber into a graduated cylinder. Therefore, the volume of the vapour phase, v_g, is:

$$v_g = v_{empty} - v_l \tag{6.6}$$

6.3.1 Non-Applicability of Raoult's Law

Since HCl-water is an azeotropic mixture, Raoult's law cannot be applied. Raoult's law assumes an ideal solution; the intermolecular forces between molecules of the same chemical species are equal to those between different species. Furthermore, Raoult's law assumes a dilute solution (low solute concentration). This assumption does not hold as $c_{HCl_{(aq)}} \rightarrow 12$ mol/L. Instead, a constant-temperature phase diagram (Pxy diagram), which can be generated in simulation software such as Chemcad, could be used to determine the concentration of the vapour phase (y_{HCl}) and of the liquid phase (x_{HCl}) based on temperature and pressure.

6.3.2 Determining x_{HCl}

The mole fraction of HCl in the liquid phase, x, can be estimated from the density of the liquid phase, ρ. A tabulation of $HCl_{(aq)}$ density in terms of concentration (weight percent HCl) and temperature is given in [46]. This tabulation is applicable for concentrations

between 1% - 40% weight percent HCl and for temperatures between -5℃ and 100℃ [46]. The concentration is converted from weight percent HCl to mole fraction HCl. A surface is then fit to the data, in MATLAB, given by:

$$\rho = 1.013 + 0.8283x - 5.057 \times 10^{-4}T \tag{6.7}$$

which can be rearranged to isolate x:

$$x = \frac{\rho - 1.013 + 5.057 \times 10^{-4}T}{0.8283} \tag{6.8}$$

where x is the mole fraction of HCl in the liquid phase, ρ is the density of the liquid phase in g/ml, and T is the temperature in ℃.

The column material is corroded by HCl. Therefore, the corrosion product, which likely contains Fe, introduces errors in the determination of ρ. The corrosion product forms an oversaturated solution with excess corrosion product settling at the bottom as precipitate, as shown in Figure 6.2. In Figure 6.2, the feed is approximately 1M $HCl_{(aq)}$. Dissolved corrosion product, as well as a precipitate settled at the bottom, are visible. The error caused by the corrosion product can be partially mitigated by decanting and filtering the liquid phase. The density of the partially-purified liquid phase is determined (from mass and volume).

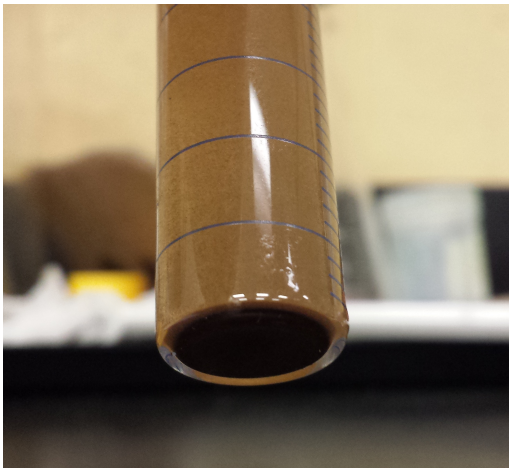

Figure 6.2: Bottoms including corrosion product.

As mentioned previously, corrosion product is clearly visible in the bottoms. However, it is not apparent in the distillate (to the unaided eye). This is possibly because the distillate is in vapour (gaseous) state when it passes by the column material. Therefore, the distillate appears clear upon condensation. While the column material is indeed corroded by HCl vapour; that vapour does not entrain or carry the corroded material. Instead, the corroded material accumulates in the bottom of the column via gravity, where it is entrained in the bottoms product, as shown in Figure 6.2.

Chapter 7

Column Geometry

7.1 Number of Stages

The number of theoretical equilibrium stages in the distillation column, N, is determined using the McCabe-Thiele method. A packed column does not have discrete plates as equilibrium stages. Therefore, a stage in a packed column is a length of packing that performs the same amount of separation as one discrete plate. This length of packing is known as height equivalent to a theoretical plate (HETP). The height of a packed distillation column, z, is given by Equation 7.1.

$$z = N \cdot HETP \tag{7.1}$$

The McCabe-Thiele method is a graphical technique to determine the required number of theoretical stages. Vertical lines are drawn on an x-y plot (a plot showing vapour concentration (y) as a function of the liquid concentration(x) corresponding to the concentrations of the feed (x_f), bottom (x_b) and distillate (x_d) products. A "staircase" is drawn between the VLE curve and the operating lines. The number of horizontal steps on the "staircase" is equal to the number of theoretical stages.

A MATLAB script, given in Appendix A.1, is written to perform the McCabe-Thiele method. The script uses tabulated data from Chemcad's PPAQ thermodyanmic model to draw the VLE curve (also called the equilibrium line) on the x-y plot. The script then plots vertical lines corresponding to the concentrations of the bottom (x_b), feed (x_f) and distillate (x_d). Finally, the script plots the operating lines (rectifying line, stripping line) and the q-line. The user must then manually draw the "staircase" and count the number of horizontal steps (i.e., theoretical stages). By application of the McCabe-Thiele method, it is determined that 9 theoretical stages are required (N = 9). Results of the McCabe-Thiele method are shown in Figure 7.1.

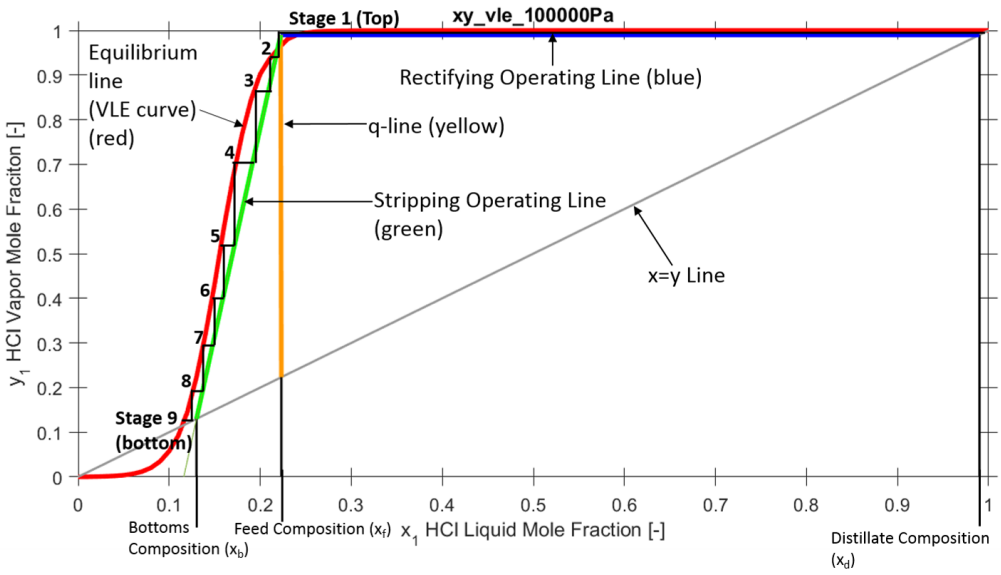

Figure 7.1: McCabe-Thiele method in MATLAB. "Staircase" is drawn manually. x_b = 0.13, x_f = 0.2232, x_d = 0.99, L_{reflux} = 0 mol/h, D = 0.05 mol/h, q = 0.999.

7.2 Column Height

The column height (z) can be determined analytically using the Method of Transfer Units (Section 7.2.1) or by using various empirical correlations (Section 7.2.2).

7.2.1 Method of Transfer Units

The variable y_i^* is the equilibrium mole fraction of vapour phase of component *i*. For a given x_i, there is a corresponding y_i on the operating line (rectifying or stripping line on the McCabe-Thiele diagram). For that given x_i, there is also a corresponding y_i^* on the equilibrium line. The equilibrium line (or VLE curve) on the x-y plot or McCabe-Thiele diagram is curve which results when Chemcad tabulated values are plotted. y_i^*, y_i and x_i are depicted in Figure 7.2. The equilbrium line shows the corresponding y_i^* (equilibrium vapour mole fraction of component *i*) for $0 \leq x_i \leq 1$ (liquid mole fraction of component *i*). The operating lines shows the corresponding y_i (vapour mole fraction of component *i*) for $0 \leq x_i \leq 1$ (liquid mole fraction of component *i*). The column height (z) can be estimated using the Method of Transfer Units, using methods and equations given in [47].

$$z = HTU \cdot NTU \tag{7.2}$$

NTU is found by integrating $1/(y_i^* - y_i)$ from y_b to y_d with respect to y.

$$NTU = \int_{y_b}^{y_d} \frac{1}{y_i^* - y_i}\, dy \tag{7.3}$$

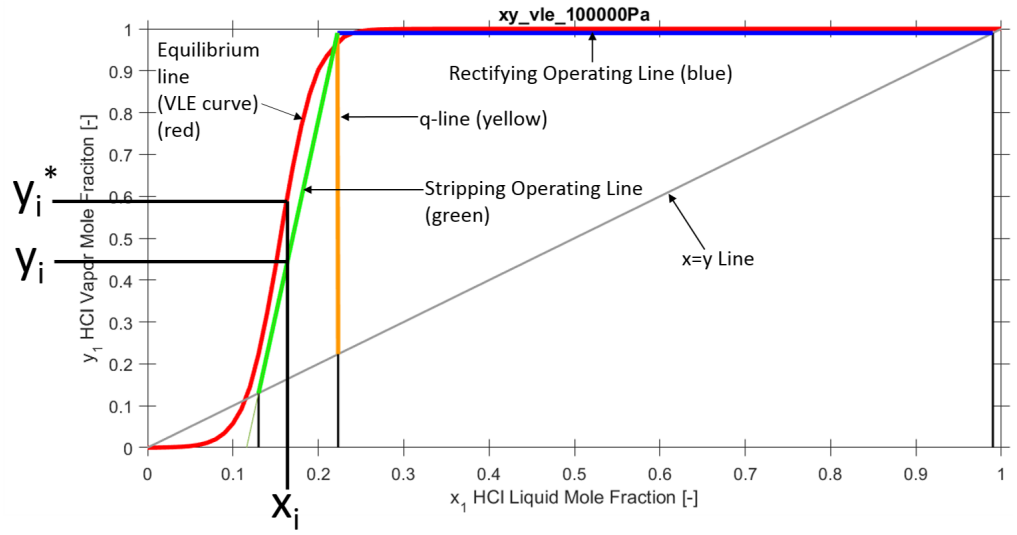

Figure 7.2: y_i^* corresponds to x_i on the *equilibrium line* (VLE curve). y_i corresponds to x_i on the *operating line*.

From Equation 7.3, it is evident that NTU is inversely related to the difference in vapour mole fractions $(y_i^* - y_i)$. This is expected since a lower $y_i^* - y_i$ indicates a lower relative volatility (graphically, the operating lines are closer to the equilibrium line). In turn, a lower relative volatility means more stages are required to perform the separation, hence a higher NTU.

Equation 7.3 is evaluated numerically in MATLAB to obtain NTU ≈ 78.

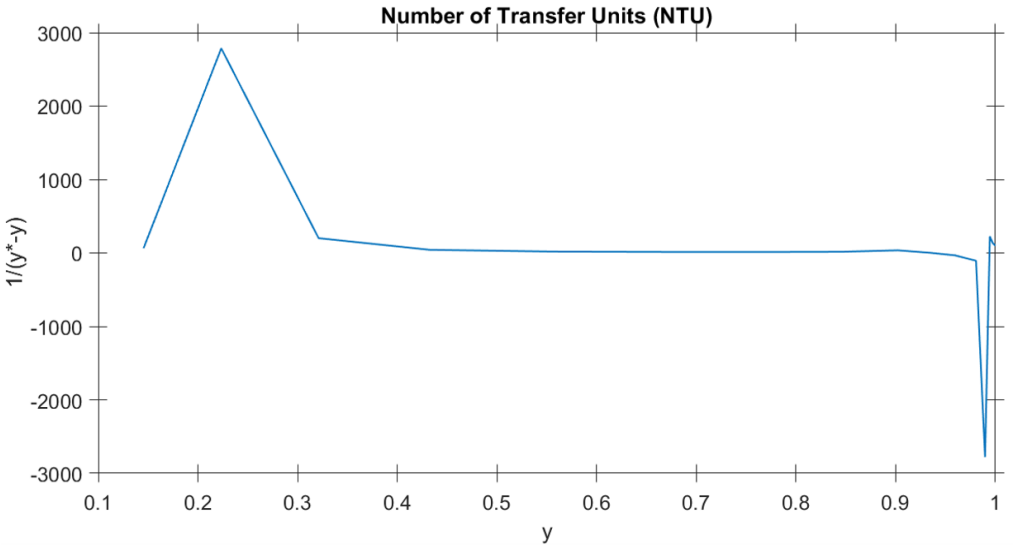

Figure 7.3: Plot of $1/(y_i^* - y_i)$ vs. y, which is numerically integrated to find NTU.

HTU is calculated using Equations 7.4 to 7.11 [47]. HTU is 0.022 m. Thus, by Equation 7.2, the column height (z) is 1.702 m. Results of the computation of Equations 7.4 to 7.11 are given in Tables 7.1 and 7.2. The diffusivity of the vapour phase (D_V) is estimated using Chapman-Enskog theory for gaseous diffusion coefficients (Equation 5.1-1 in [48]), as shown in Equation 7.9 and Table 7.2.

$$d_e = 4\frac{\varepsilon}{\omega} \tag{7.4}$$

$$Ar = \frac{d_e^3(\rho_L - \rho_V)\rho_V g}{\nu_v^2} \tag{7.5}$$

$$Re = 0.15 \cdot Ar^{0.57}\left(\frac{V}{L}\right)^{0.43} \tag{7.6}$$

$$v_v = \frac{Re\,\nu_v}{d_e\,\rho_v} \tag{7.7}$$

$$K_V = \frac{0.35\,Re^{0.8}\left(\frac{\nu_V}{\rho_v D_V}\right)^{0.35} \cdot D_V}{d_e^2} \tag{7.8}$$

$$D_V = \frac{1.86\ \cdot 10^{-3}\,T^{3/2}\sqrt{\frac{1}{MM_{HCl}} + \frac{1}{MM_{H_2O}}}}{P\sigma_{HCl-H_2O}^2\,\Omega} \tag{7.9}$$

$$\sigma_{HCl-H_2O} = \frac{1}{2}\left(\sigma_{HCl} + \sigma_{H_2O}\right) \tag{7.10}$$

$$HTU = \frac{v}{K_V} \tag{7.11}$$

7.2.2 Empirical Correlations

As mentioned in Section 3.7, the work of Wang et al [34] includes an aggregation of empirical HETP correlations for packed columns from numerous researchers. These correlations give HETP in terms of various parameters such as phase densities, phase velocities, phase dynamic viscosities and column diameter. The column height (z) can also be expressed by Equation 7.1. The work of Wang et al [34] includes an aggregation of empirical correlations (i.e., "shortcut" methods) for HETP from various researchers [49–53]. The researchers corresponding to each correlation are cited in Wang et al [34]. Values used to calculate the correlations are given in Table 7.3. Results of these empirical correlations are tabulated in Table 7.4.

The HETP correlation of Ellis, [49] via [34], is given by Equation 7.12.

$$HETP = \left[18\,d_e + 0.305\,m_{eq}\left(\frac{\rho_G u_G}{\rho_L u_L} - 1\right)\right]\left(\frac{Z_p}{3.05}\right)^{0.5} \tag{7.12}$$

Table 7.1: Parameters for Calculating HTU

Quantity	**Value**	**Comment**
HTU [m]	0.022	Computed via Equation 7.11.
NTU [-]	78.0939	Estimated in MATLAB by numerically integrating the curve in Figure 7.3.
z [m]	1.702	Computed via Equation 7.2.
d_e [m]	4.06×10^{-3}	Computed via Equation 7.4.
ε [m^3/m^3]	0.8	User assumed parameter.
ω [m^2/m^3]	789	Calculated based on the geometry of a Raschig ring.
Ar [-]	514096	Computed via Equation 7.5.
ρ_G [kg/m^3]	1.415	
ρ_L [kg/m^3]	774.6	
ν_V [kg/m·s]	3.73×10^{-5}	Estimated in EES.
Re [-]	270.0	Computed via Equation 7.6.
L [kmol/h]	0.001	User assumed parameter.
V [kmol/h]	0.001	User assumed parameter.
v_v [m/s]	1.76	Computed via Equation 7.7.
K_V [1/s]	80.55	Computed via Equation 7.8.
D_V [m^2/s]	5.586×10^{-5}	Estimated using Chapman-Enskog theory. See equation Equation 7.9, Equation 7.10 & Table 7.2.

Table 7.2: Parameters used in Equation 7.9 to Calculate D_V

Quantity	**Value**
D_V [m^2/s]	5.586×10^{-5}
MM_{HCl} [g/mol]	36.46
MM_{H_2O} [g/mol]	18.02
P [atm]	1
T [K]	339
σ_{HCl} [Å]	2.14
σ_{H_2O} [Å]	2.75
$\sigma_{HCl\text{-}H_2O}$ [Å]	2.45
Ω [-]	1

Table 7.3: Values used to Calculate Empirical Correlations for HETP

Quantity	**Value**	**Comment**
ρ_G [kg/m^3]	1.415	From EES.
ρ_L [kg/m^3]	774.6	Computed in EES as weighted average by mole fractions in the liquid phase.
u_G [m/s]	1.76	User assumed parameter.
u_L [m/s]	1	User assumed parameter.
a_P [m^2/m^3]	789	Calculated based on the geometry of a Raschig ring.
Φ [m]	0.0114	Calculated in Section 7.3.
m [-]	1.13080	Constant from Table 7-2 in [52] for 1 in Pall rings, since the table does not list Raschig rings.
ν_L [kg/(m·s)]	3.38×10^{-4}	Computed based on EES data @ T = 339K, P = 101.325 kPa.
σ_L [N/m]	0.05087	From EES.

Table 7.4: Results of Empirical Correlations for HETP

Empirical Correlation	**HETP [m]**
Ellis [49] via [34]	0.730
Harrison and France [50] via [34]	0.127
Kister [51] via [34]	0.229
Strigle [52] via [34]	0.985
Lockett [53] via [34]	0.174

The HETP correlation of Harrison and France, [50] via [34], is given by Equation 7.13.

$$HETP = \frac{100}{a_p} \tag{7.13}$$

The HETP correlation of Kister, [51] via [34], is given by Equation 7.14.

$$HETP = \frac{100}{a_p} + 0.102 \tag{7.14}$$

The HETP correlation of Strigle (for $0.4\,atm \leq P \leq 4\,atm$; $4\,mN/m \leq \sigma_L \leq 36\,mN/m$; $0.08\,cP \leq \nu_L \leq 0.83\,cP$), [52] via [34], is given by Equation 7.15. The symbol m represents a dimensionless constant associated with the packing, m = 1.13080 for 1 in. Pall rings (Table 7-2 in [52], Raschig rings are not listed).

$$HETP = exp\,(m\ -\ 0.187\,ln\,(\sigma_L)\ +\ 0.213\,ln\,(\nu_L)) \tag{7.15}$$

The HETP correlation of Lockett, [53] via [34], is given by Equation 7.16.

$$HETP = \frac{1.54 g^{0.5}\,(\rho_L\ -\rho_g)^{0.5}\,\nu^{-0.06}}{a_p\,[1\ +\ 0.78\,exp(0.00058 a_p)(\rho_g/\rho_L)^{0.25}]^2} \tag{7.16}$$

7.3 Column Diameter

An algorithm to estimate internal column diameter (Φ) is given in [47], as shown in Equations 7.17 to 7.19. Generally, a larger column diameter corresponds to a larger maximum allowable mass flow rate (of feed, distillate and bottoms). Results of the computation of Equations 7.17 to 7.19 are given in Table 7.5.

$$\Phi = \sqrt{\frac{3 \cdot W_V}{\pi \cdot v_v}} \tag{7.17}$$

$$log \frac{v_0^2 \omega \rho_v \nu_L^{0.16}}{g \epsilon^3 (\rho_L - \rho_V)} = -0.125 - 1.75 \left(\frac{L}{V}\right)^{0.25} \left(\frac{\rho_V}{\rho_L - \rho_V}\right)^{0.125} \tag{7.18}$$

$$v_v = 0.6 \cdot v_0 \tag{7.19}$$

7.4 Location of Feed Stage

The location of the feed stage (i.e., at which stage the feed is input) is determined based on feed concentration. The feed stage is the stage (horizontal step on the "staircase") which is above the feed concentration. The column is designed such that the feed stage can be moved discretely along the column depending on feed concentration.

Table 7.5: Parameters for Calculating Column Diameter

Quantity	**Value**	**Comment**
Φ [m]	0.0114	Computed via Equation 7.17.
W_V [m^3/s]	1.00×10^{-4}	User assumed parameter.
v_v [m/s]	0.73	Computed via Equation 7.19.
v_0 [m/s]	1.22	Computed via Equation 7.18.
ϵ [-]	0.8	User assumed parameter.
ρ_L [kg/m^3]	774.6	Computed in EES with T = 339 K.
ρ_G [kg/m^3]	1.415	Computed in EES with T = 339 K.
ω [m^2/m^3]	789	Calculated based on the geometry of a Raschig ring.
ν_L [Pa·s]	3.38×10^{-4}	Computed in EES with T = 339 K, P = 101.325 kPa.
L [kmol/h]	0.001	User assumed parameter.
V [kmol/h]	0.001	User assumed parameter.

Chapter 8

Measurement and Control

8.1 Temperature Measurement

As shown in Figure 8.1, the centerline temperatures at the zone midpoints are measured via T-type thermocouples, and the pipe exterior wall temperatures at the boundaries between zones are measured via J-type thermocouples.

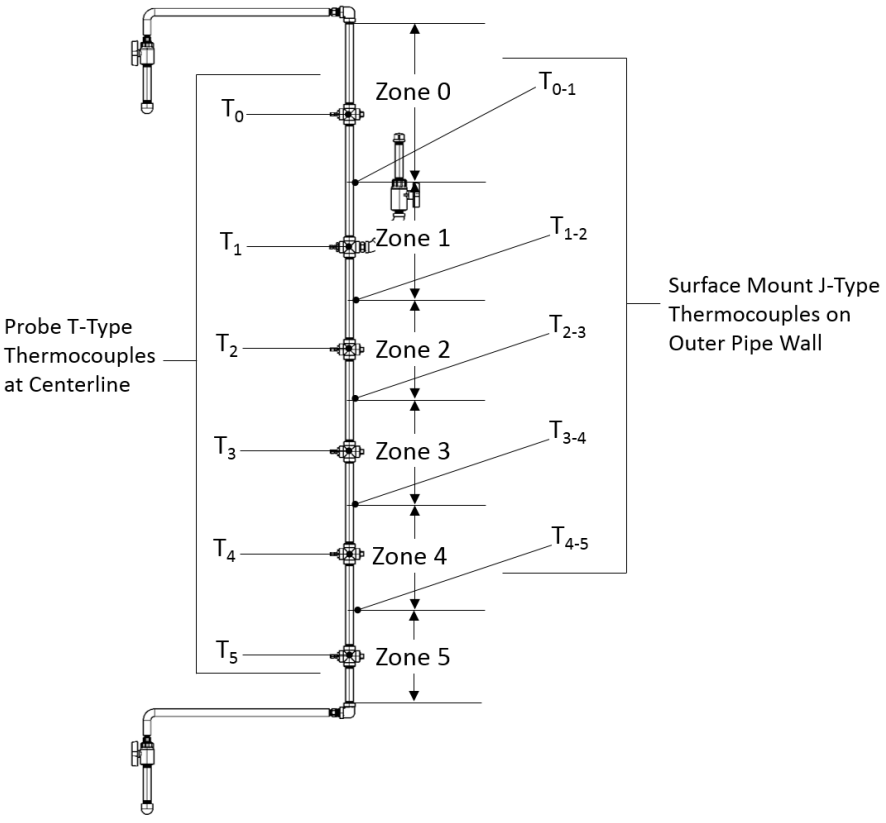

Figure 8.1: Thermocouple locations and temperature zones.

8.2 Column Heating

The column is heated via six 125 W heating tapes (one per temperature zone, total: 750 W), wrapped helically around the exterior of the column. Heat is transferred to the column interior via conduction through the walls. To minimize heat loss, zones 2-5 are wrapped with fiberglass insulation. The column energy balance is as follows:

$$\begin{aligned} \sum E_{in} &= \sum E_{out} \\ Q + h_f &= h_b + h_d \end{aligned} \tag{8.1}$$

The distillation involves two components; in the most general case, each component exists in two phases, for a total of four entities: $H_2O_{(g)}$, $H_2O_{(l)}$, $HCl_{(g)}$ and $HCl_{(aq)}$.

The two chemical species (HCl & H_2O) cannot be treated separately because HCl dissolves in H_2O. The thermophysical and thermochemical properties of $HCl_{(aq)}$ are different than those of both $HCl_{(l)}$ and $H_2O_{(l)}$. Therefore, the enthalpies of the feed, distillate, and bottoms streams (h_f, h_b, h_d; respectively) are found via Chemcad's property calculator. Values of h are negative due to Chemcad's selection of the reference state. Column heat input (Q) is calculated via Equation 8.1. It is unfeasible to perform the property calculations for h_f, h_b and h_d in EES, as EES does not support $HCl_{(aq)}$. EES also returns a fatal error when a temperature argument in a property calculation exceeds a component's critical temperature. Chemcad does not suffer these limitations. The time (t) required, per mole of feed, for the column to reach operating temperature is calculated by Equation 8.2. The heating tapes are assumed to have 100% energy efficiency because they are ohmic (resistance) heaters. More heating tapes (larger $\dot{Q}$) would result in a shorter heating time per mole of feed (t). Calculation results are tabulated in Table 8.1.

It is assumed that all the energy emitted from the heating tape is used to heat the column. However, not all the heat from the tape goes to the column (e.g., some heat goes to the ambient air), therefore, the heating time per mole of feed (t) is longer than that predicted by Equation 8.2.

$$t = \frac{Q}{\dot{Q}} \tag{8.2}$$

8.3 Control System

8.3.1 Schmitt Trigger

A LabView program is used to maintain column axial temperature profile. T-type thermocouples are used as analog inputs to LabView to measure temperature. The NI

Table 8.1: Parameters for Calculating Column Heat Input

Quantity	**Value**	**Comment**
x_d [-]	0.99	
x_f [-]	0.2232	
x_b [-]	0.13	
T_d [K]	298	Assumed, T_d is near $T_{ambient}$ since $m_{ambient\ air} \gg m_d$.
T_f [K]	350	
T_b [K]	375	
h_d [J/mol]	-9.43×10^4	Data from Chemcad.
h_f [J/mol]	-2.51×10^5	Data from Chemcad.
h_b [J/mol]	-2.65×10^5	Data from Chemcad.
Q [J/mol]	-1.08×10^5	Calculated via Equation 8.1.
$\dot{Q}$ [W]	750	Given in heating tape data.
t [s/mol]	144.2	Calculated via Equation 8.2.

9472 digital output module generates a binary (on/off) control signal, according to the LabView program, which is used to switch relays. The relays, in turn, switch heating tapes. A control diagram is shown in Figure 8.2. A Schmitt trigger is implemented in the LabView program to prevent high-frequency oscillation of the control signal. The thresholds of the Schmitt trigger are defined in Equations 8.3 and 8.4. A lower offset moves the thresholds closer together, which results in less deviation from the setpoint (i.e., less error) but increases the frequency of oscillation. A flowchart of the Schmitt trigger is shown in Figure 8.3.

The Schmitt trigger resulted in large amplitude osciallations about the setpoint. Therefore, it is abandoned in favor of proportional control.

$$Upper\ threshold = Setpoint + Offset \tag{8.3}$$

$$Lower\ threshold = Setpoint - Offset \tag{8.4}$$

8.3.2 PID Control

Since a Schmitt trigger is inadequate for maintaining the temperature near a setpoint, PID control (proportional, integral, differential) is used to maintain the temperature of a zone at a setpoint with minimal fluctuation (oscillation amplitude) and minimal error (difference between setpoint and process variable (e.g., temperature)). Error is given by Equation 8.5. A flowchart of PID control is given in Figure 8.4. The power of a heating tape is varied by changing the duty cycle of pulse-width modulation (PWM). A

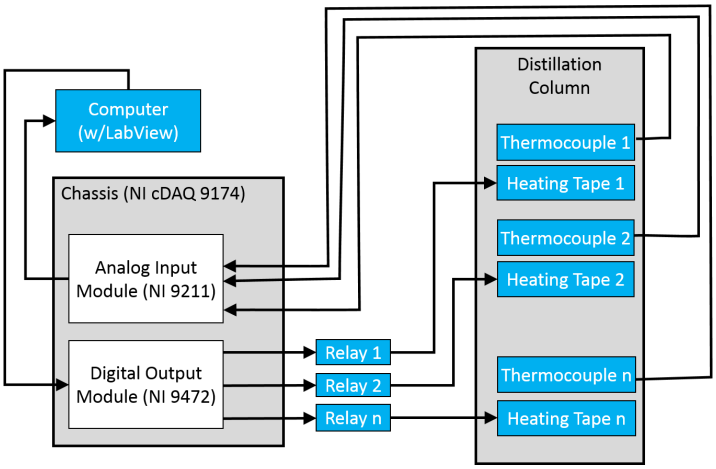

Figure 8.2: Control diagram for n temperature zones.

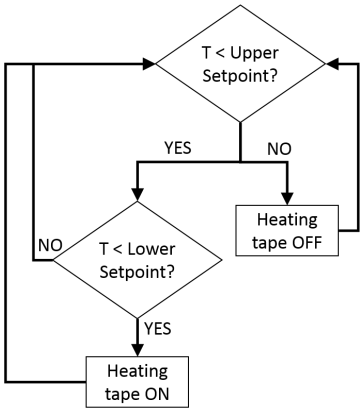

Figure 8.3: Schmitt trigger flowchart.

PWM period of 20 seconds is selected to decrease the prevalence of rapid switching of the mechanical relays, which leads to their premature failure.

$$e(t) = r(t) - y(t) \tag{8.5}$$

where:

- e(t) is the error at time t,
- r(t) is the setpoint at time t,
- y(t) is the process variable at time t (in this case, y(t) is temperature [°C]).

PID control is described by Equation 8.6:

$$u(t) = k_p e(t) + k_i \int_0^t e(\tau)\,\mathrm{d}\tau + k_d \frac{de}{dt} \tag{8.6}$$

where:

- u(t) is the control signal at time t (in this case, u(t) is the heater duty cycle [%], which is analogous to heater power),
- e(t) is the error,
- τ is the time over the integral bounds, that is, τ varies from 0 to t,
- k_p is the proportional gain,
- k_i is the integral gain,
- k_d is the derivative gain.

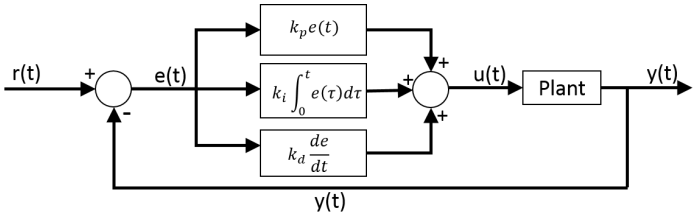

Figure 8.4: PID control flowchart.

The PID gains (k_p, k_i, k_d) are determined via trial-and-error and via the Ziegler-Nichols method. The processes of determining gains, by any method(s), is known as tuning.

The Ziegler-Nichols method requires the ultimate gain, k_u, that is, the proportional gain at which the system begins to be unstable (i.e., exhibits unbounded oscillation). k_u can be determined empirically, by gradually increasing k_p until unbounded oscillation is observed, or analytically, for example, by using the Routh stability criterion. The Ziegler-Nichols method also requires T_u, the period of oscillation at k_u. Once k_u and T_u are known, k_p, k_i, and k_d are computed from a Ziegler-Nichols tuning chart [54].

Tuning k_p reduces the rise time. That is, it causes the process variable to reach its setpoint more quickly. However, if k_p is too large, steady oscillation or even unbounded oscillation of the process variable, y(t), may occur. Tuning k_i reduces or eliminates error at steady-state (offset). Tuning k_d reduces or eliminates overshoot.

Since the system heats fluids through a temperature change (sensible heating), as well as a phase change (latent heating), the overall relation between temperature (T) and heat input (Q), dT/dQ, is not linear. The rate dT/dQ can be assumed linear for sensible heating only. For phase change, $dT/dQ = 0$, because phase changes are isothermal. To provide sufficient heat to complete a phase change, k_p must be set fairly high ($10 \leq k_p \leq 20$). However, such a high value of k_p results in large overshoot. A workaround

is to manually decrease k_p immediately after a phase change is finished (i.e., when the temperature begins to increase again), or shortly before a phase change is estimated to finish. More accurate control would result if u(t), the control signal (duty cycle), is calculated based on enthalpy instead of temperature, however, there are no devices available that directly measure enthalpy.

For the insulated zones (zones 2-5), k_p is initially approximately 11; when the phase change (boiling) is nearly complete, k_p is decreased to approximately 7. For the uninsulated zones (zones 0-1), k_p is initially between 15 and 25; when the phase change (boiling) is nearly complete, k_p is decreased to approximately 10. The variable k_p is higher for the uninsulated zones since a higher duty cycle is required because the rate of heat loss is greater.

It is determined that proportional control alone is adequate for the purpose of this research, therefore, $k_i = k_d = 0$. Integral control is not necessary because a few ℃ of steady-state error (offset) is allowable. Derivative control is also unnecessary because overshoot is permissible (i.e., the materials can withstand the higher temperatures that occur during overshoot), simply more time is required for the temperature zone to reach steady-state.

The transfer function, H(s), of an element in a control system (e.g., controller, plant) is given by Equation 8.7.

$$H(s) = \frac{Y(s)}{X(s)} \tag{8.7}$$

where:

- Y(s) is the Laplace transform of the output, y(t),
- X(s) is the Laplce transform of the input, x(t).

The Laplace transform maps a function of t (time) to a function of s (complex frequency, $s = \sigma + j\omega$), as shown by Equation 8.8.

$$\mathscr{L}\{f(t)\} = F(s) \tag{8.8}$$

The input is an approximated impulse. That is, one heating tape is run at 100% duty cycle (125 W) for $t \leq 25$ s, then at 0% duty cycle for $t > 25$ s. All other heating tapes are held constant at 0% duty cycle. This input may be considered an impulse since 25 s is negligible relative to the duration of observation (> 1 hr).

To reduce column start-up time (time required for all zones to be stabilized at their setpoints), it is found that the heating tapes should be started in order of decreasing temperature (i.e., those with the hottest setpoints should be started earlier). This will

minimize the overheating (when T > SP) of zones with colder setpoints. Otherwise, due to the heat transfer through adjacent zones, the zones with colder setpoints will get vastly overheated and will require much time to cool to their setpoints, thus increasing start-up time. If the heating tapes are started in order of decreasing temperature, by the time the hottest zones are stabilized at their setpoints, the zones with colder setpoints may already be inadvertently heated to near (or even above) their setpoints (due to heat transfer through adjacent zones) and thus will require little to no heat from their own heating tapes.

8.3.3 Electrical Design

As mentioned in Section 8.3, relays (AutomationDirect 781-1C-24D) are used to switch the heating tapes. The NI 9472 digital output module (which is controlled by the LabView program) drives the relay coils. The NI 9472 cannot switch the heating tapes directly because it is rated for a maximum of 30 VDC and 0.75 A/channel [55]. Whereas, the heating tapes require 120 VAC and 1.0 A to 5.3 A (depending on the power consumption of the tape). Therefore, each relay is controlled by the NI 9472, which switches 24 VDC (coil side). In turn, the relays switch the heating tapes at 120 VAC (contact side). An advantage of using relays in this manner is that they isolate the AC & DC circuits. For example, if a fault, such as a current spike caused by a short, occurs in an AC circuit; the current spike would not be transmitted to the DC circuit (which includes expensive and sensitive equipment such as the NI 9472 and NI cDAQ-9174).

A critical part of the relays are the coils, which are inductors. A flyback diode (1N4007) is installed in parallel with each relay to dissipate the voltage spike that occurs when the relay's coil circuit is open. When the current flows through the relay coil (closed coil circuit), the coil (an inductor) stores energy in a magnetic field. When the coil circuit is open, the coil's polarity is reversed and the energy that was stored in the magnetic field in the coil is released as a voltage spike, as given by Equation 8.9 [56]. Since the flyback diode is present, the energy of the voltage spike is dissipated in the diode. If no flyback diode was present, the voltage spike could enter sensitive equipment in the circuit, potentially causing damage to it. The voltage stored in an inductor is given as:

$$V = L\frac{dI}{dt} \tag{8.9}$$

where V is voltage [V], L is inductance [H], I is current [A], and t is time [s].

Furthermore, fusible disconnect switches, comprising 10 A fuses, are installed on the AC circuits. They can be operated as regular switches; however, they also comprise a fuse, which melts if the current exceeds the rating (e.g., as would occur during a short),

thereby interrupting the current. The fuses are separable from the disconnect switch, so only the fuse is replaced after a fault. A schematic of the electrical system used to measure and control column temperature is given in Figure 8.5.

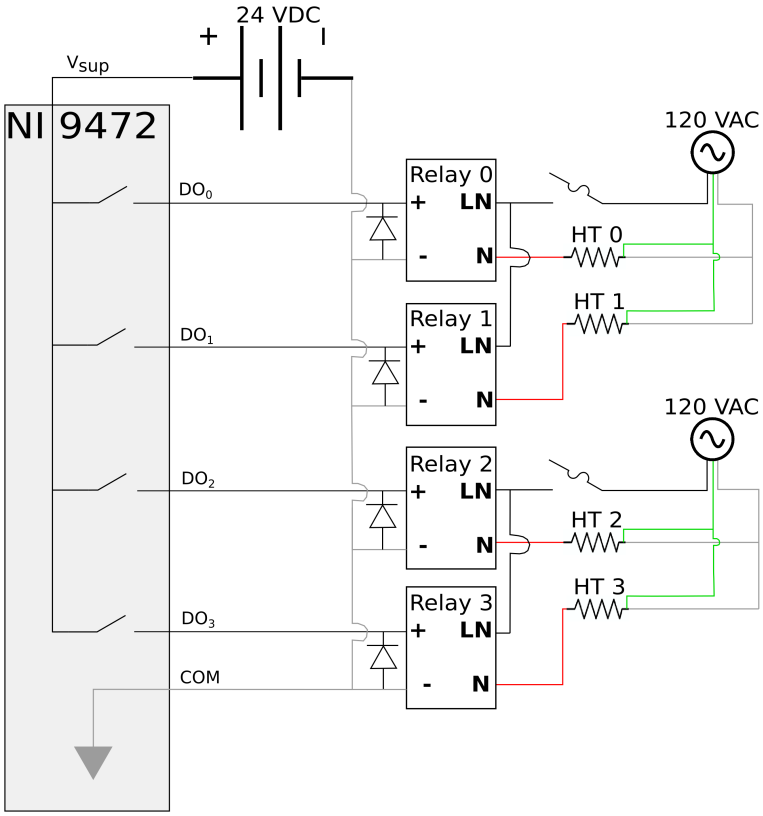

Figure 8.5: Electrical control schematic.

Chapter 9

Apparatus Operation

9.1 Experimental Procedure

Connect the output ports to the output chambers via hoses. Ensure all connections are air-tight. Open output chamber valves. Close feed chamber valve.

Prepare $HCl_{(aq)}$ solution of desired molarity at room temperature, inside the fume hood. **Always pour acid into water**, thereby gradually increasing the concentration of $HCl_{(aq)}$ from zero. If water is added into acid (dangerous): initially, the resulting solution will have a high concentration of $H^+{}_{(aq)}$ & $Cl^-{}_{(aq)}$ ions. Since the solution has a high concentration of these ions, a lot of hydration of these ions will occur. Hydration is highly exothermic; the released heat may cause the solution to boil rapidly and splatter violently. However, if acid is added to water (the safe method), there are initially few $H^+{}_{(aq)}$ & $Cl^-{}_{(aq)}$ ions present to undergo hydration. Much less heat is released, because much less hydration occurs. The logic is thus: low ion concentration $\rightarrow$ fewer ions avaliable for hydration $\rightarrow$ less hydration $\rightarrow$ less heat released.

Ensure feed chamber valve is closed. Open feed chamber cap, inject solution into feed chamber using syringe, close feed chamber cap. Using the LabView VI, enter proportional gains and temperature setpoints, run VI. Allow column to reach operating temperatures. Once column has reached steady-state operating temperature(s), open feed chamber valve (leave cap closed). Close valve once chamber is empty.

Allow distillation to run. Distillation is complete when all of the feed mixture is separated (i.e., output chambers are no longer filling). Fluid flow into the output chambers can be seen through the semi-transparent hoses which connect the column to the feed chambers. Once distillation is complete, close output chamber valves.

Unplug electrical controls. Stop LabView VI. Allow column to cool to a safe temperature before touching it. Once the column is at a safe temperature, ensure that the

output chamber valves are closed, disconnect the output chambers from the column, and analyze the chambers as per the procedure described in Section 6.3. Dispose of hazardous solvents, solutions, mixtures, and reaction residues as hazardous waste. Clean up work area and lab equipment. Any $HCl_{(aq)}$ spills should be cleaned promptly with absorbent. Used absorbent should be disposed as hazardous waste.

Chapter 10

Distillation Experimental Results and Discussion

10.1 Analysis of the Column Outputs

Based on the calculated results (Table 10.1), the column appears to be separating the mixture components as expected. That is, the distillate contains less hydrogen chloride than the feed, and the bottoms contains more hydrogen chloride than the feed. The concentration of hydrogen chloride in bottoms is still less than azeotropic (0.11 mole fraction of hydrogen chloride). This is expected as it is not possible to distill through the azeotrope using only simple distillation. Doing so is impossible, because at the azeotropic concentration (0.11 mole fraction of hydrogen chloride), the concentration (i.e., mole fraction) of hydrogen chloride in the liquid phase is equal to that in the vapour phase.

The results of column operation are given in Table 10.1. The approximate molarity of the feed solution, $\sim c_{feed}$, is provided. However, due to slight errors in solution preparation, the actual mole fraction of HCl molecules in the feed, x_{feed}, is also calculated and provided. For purposes of analysis, x_{feed} should be used instead of $\sim c_{feed}$, as the former more accurately represents the concentration of HCl molecules in the feed solution. The mole fraction of HCl in the distillate and bottoms, $x_{column\ output}$, is calculated from ρ and T using Equation 6.8. $x_{column\ output}$ refers collectively to $x_{distillate}$ and $x_{bottoms}$.

The experiment numbers are integers assigned by the LabView program. They are incremented by +1 each time the LabView program is run. Their magnitude is arbitrary; however, they serve to identify individual experiments. The letters D and B after the experiment numbers signify distillate and bottoms, respectively.

The distillate (D) from all experiments is calculated to have a mole fraction of HCl of 0, which suggests that the distillate is virtually pure $H_2O_{(l)}$.

Table 10.1: Measured Densities and Calculated Concentrations

Experiment Number	$\sim c_{\text{column feed}}$ **[mol/L]**	$x_{\text{column feed}}$ **[mol/mol]**	ρ **[g/ml]**	$x_{\text{column output}}$ **[mol/mol]**
385D	1	0.0180	0.979	0
385B	1	0.0180	1.036	0.0400
386D	2	0.0362	0.966	0
386B	2	0.0362	1.058*	0.0655
387D	1	0.0191	0.970	0
387B	1	0.0191	1.091*	0.1068
388D	0.5	0.0099	0.970	0
388B	0.5	0.0099	1.048*	0.0547
389D	3	0.0549	0.966	0
389B	3	0.0549	1.072*	0.0832
391D	0.5	0.0095	0.953	0
391B	0.5	0.0095	1.080*	0.0944
392D	2	0.0368	0.967	0
392B	2	0.0368	1.076*	0.0896
*Calculated after one or more filtrations. Filtration is necessary because of the corrosion product, as described in Section 6.3.2.				

The composition of the bottoms (B) from the experiments varies considerably from experiment to experiment. A possible reason for this variation is explained in Section 10.2.1. However, in all experiments the bottoms is calculated to have a mole fraction of HCl less than 0.11 (the azeotropic concentration). This is expected as it is impossible to cross the azeotrope with a single pressure; because at the azeotrope, the vapor and liquid phases are of identical composition.

From the results given in Table 10.1, it appears that the column is separating the mixture components such that:

$$0 \leq x_{\text{distillate}} < x_{\text{feed}} < x_{\text{bottoms}} < x_{\text{azeotropic}}, \quad \text{where } x_{\text{azeotropic}} = 0.11 \text{ mol/mol} \tag{10.1}$$

This means that the column is partially separating the mixture such that the distillate has less HCl than the feed, the bottoms has more HCl than the feed, and all three streams (feed, bottoms, distillate) are of a concentration less than azeotropic.

10.1.1 Comparison of Experimental Results and Simulation Results

As shown by Table 10.2, there is reasonable agreement between the experimental and simulation results. All experiments and simulations in Table 10.2 satisfy the criterion of Equation 10.1.

However, there are discrepancies between the experimental x_{output} and the simulated x_{output} for similar feed concentrations. For example, identifier 388 and identifier 1 have similar feed concentrations. Yet for experimental, $x_{\text{bottoms } 388} = 0.0547$, whereas, for simulated, $x_{\text{bottoms } 1} = 0.03$. The experimental output concentration is approximately 1.8 times the simulated output concentration, despite very similar feed concentrations. This discrepancy may be due to the fact that the experimental unit is a packed column whereas the simulated unit is a perforated-plate column. Furthermore, the simulated unit may be of insufficient length (i.e., not enough plates) to achieve the maximum possible degree of separation.

10.2 Weaknesses & Limitations in the Results

10.2.1 Corrosion Product

The considerable variation in mole fraction of HCl for the bottoms is likely due to the presence of corrosion product (Figure 6.2). The presence of corrosion product affects the calculation of the density, ρ, which in turn affects the determination of the mole fraction of HCl in the distillate or bottoms, x_{output}. Any output product, the distillate or bottoms, can only be filtered a finite number of times, as the filter absorbs some liquid each time a liquid is poured through it. Thus, the mass that leaves the filter is less than the mass that enters it.

10.2.2 Vapour Pressure of the Vapour Phase

It is not feasible to analyze y, the mole fraction of HCl in the vapour phase, as the vapour pressure of $HCl_{(aq)}$ is ≤ 0.04 kPa at the concentrations (< 7 mol/L) and temperatures (approximately 20 °C) in question, according to Fritz [57]. Pressure gages of the required sensitivity are not available at the time of experimentation.

Table 10.2: Comparison of Experimental Results and Simulation Results

	Identifier	$\mathbf{x_{feed}}$ **[mol/mol]**	$\mathbf{x_{output}}$ **[mol/mol]**
Experimental	385D	0.0180	0
	385B	0.0180	0.0400
	386D	0.0362	0
	386B	0.0362	0.0655
	387D	0.0191	0
	387B	0.0191	0.1068
	388D	0.0099	0
	388B	0.0099	0.0547
	389D	0.0549	0
	389B	0.0549	0.0832
	391D	0.0095	0
	391B	0.0095	0.0944
	392D	0.0368	0
	392B	0.0368	0.0896
Simulation	1D	0.01	0.00
	1B	0.01	0.03
	2D	0.03	0.00
	2B	0.03	0.10
	3D	0.05	0.03
	3B	0.05	0.11
In the 2nd column, D and B signify distillate and bottoms, respectively.			

Table 10.3: Instrument Uncertainties

Description	**Manufacturer Info**	**Uncertainty**
T-Type Thermocouple	Omega CPIN-18U-12	± max(1.0 ℃ , 0.75%) [58]
J-Type Thermocouple	Omega 5TC-GG-J-30-72	± max(2.2 ℃ , 0.75%) [58]
Mechanical Temperature Gage	Winters	± 1 ℃*
Balance	Mettler Toledo PB3002-S	± 0.005 g* [59]
Balance	Mettler Toledo AB204-S	± 5×10^{-5} g*
50ml & 100ml Graduated Cylinders	Kimax Kimble	± 0.5 ml*
10ml Graduated Cylinder	Kimax Kimble	± 0.1 ml*
*Where uncertainty is not explicitly stated by the manufacturer, it is taken to be ± half of the smallest gradation [60]. The smallest gradation is determined, for example, by observing the tick marks on a gage or graduated cylinder, or the smallest increment on the digital display of a balance.		

10.3 Uncertainty Analysis

10.3.1 Systematic Error

Sources of systematic error include:

- Corrosion product in the liquid phase of the bottoms output causes the density to be overstated. This error can be partially mitigated by filtration, but cannot be quantified, by differential mass, because the filter paper absorbs liquid in addition to the precipitate.
- Errors in temperature control:
  - Temperature oscillation around the setpoint,
  - Temperature steady-state error (offset),
  - Temperature overshoot.
- Spillage from hoses when they are disconnected from the output chambers. This causes the volume of the distillate the bottoms to be understated.
- The HCl-H_2O phase diagram (e.g., the azeotropic concentration [mol/mol], bubble points [℃], and dew points [℃]) changes slightly with pressure, as shown in Figure 5.2.

10.3.2 Random Error

Sources of random error include:

- Fluctuations in the ambient temperature of the room, which affects the heat duty.

10.3.3 Method of Kline & McClintock

The method of Kline & McClintock [61] is used to determine the uncertainty of a calculated value whose arguments are measured from physical devices. A MATLAB script, given in Appendix A.2, is written to perform the method of Kline & McClintock.

According to Kline & McClinotck [61], for a calculated result, R, which is calculated from the measured independent variables, x_1, x_2,...,x_n, then the uncertainty of that result, w_R, is:

$$w_R = \left[\left(\frac{\delta R}{\delta x_1} w_1 \right)^2 + \left(\frac{\delta R}{\delta x_2} w_2 \right)^2 + ... + \left(\frac{\delta R}{\delta x_n} w_n \right)^2 \right]^{1/2} \tag{10.2}$$

where:

- x_1, x_2,...,x_n are the independent variables of which R is a function, i.e., R = f(x_1, x_2,...,x_n). The values of x_1, x_2,...,x_n are physically measured using instruments.
- w_n is the uncertainty of independent variable x_n (e.g., the given uncertainty of an instrument),
- R is the calculated result,
- w_R is the uncertainty of the calculated result.

Uncertainties determined via the method of Kline & McClintock (calculated via the MATLAB script given in Appendix A.2) are given in Table 10.4. The letters D and B after the experiment numbers signify distillate and bottoms, respectively. Table 10.4 also shows the maximum and minimum output product concentrations that occur due to the uncertainties. These maximum and minimum output product concentrations are calculated as:

$$\text{Maximum Output Product Concentration} : \; x_{output,\,max} = x_{output} + w_{x_{output}} \tag{10.3}$$

$$\text{Minimum Output Product Concentration} : \; x_{output,\,min} = x_{output} - w_{x_{output}} \tag{10.4}$$

The variables $x_{output,\,max}$ and $x_{output,\,min}$ give the maximum and minimum values of x_{output}. They are computed by Equation 10.3. The resulting range in the value x_{output} is caused by uncertainties in measurement (instrument uncertainty) and calculation. Of course, it is not possible that $x_{output} < 0$. Whenever this occurs, x_{output} should be floored to zero. As discussed earlier, it is not possible to cross the azeotrope, therefore, when $x_{output} > 0.11$, it should be capped to 0.11.

Table 10.4: Uncertainties, following the approach of Kline & McClintock

Experiment Number	$\mathbf{w_{x_{feed}}}$ **[mol/mol]**	$\mathbf{w_{\rho}}$ **[g/ml]**	$\mathbf{w_{x_{output}}}$ **[mol/mol]**	$\mathbf{x_{output,\ min}}$ **[mol/mol]**	$\mathbf{x_{output,\ max}}$ **[mol/mol]**
385D	$\pm 2.115\times10^{-5}$	$\pm$ 0.0122	$\pm$ 0.0148	-0.0148	0.0148
385B	$\pm 2.115\times10^{-5}$	$\pm$ 0.0123	$\pm$ 0.0149	0.0251	0.0549
386D	$\pm 2.102\times10^{-5}$	$\pm$ 0.0112	$\pm$ 0.0136	-0.0136	0.0136
386B	$\pm 2.102\times10^{-5}$	$\pm$ 0.0132	$\pm$ 0.0160	0.0495	0.0815
387D	$\pm 2.103\times10^{-5}$	$\pm$ 0.0099	$\pm$ 0.0120	-0.0120	0.0120
387B	$\pm 2.103\times10^{-5}$	$\pm$ 0.0123	$\pm$ 0.0149	0.0919	0.1217
388D	$\pm 2.116\times10^{-5}$	$\pm$ 0.0110	$\pm$ 0.0133	-0.0133	0.0133
388B	$\pm 2.116\times10^{-5}$	$\pm$ 0.0125	$\pm$ 0.0151	0.0396	0.0698
389D	$\pm 2.100\times10^{-5}$	$\pm$ 0.0138	$\pm$ 0.0167	-0.0167	0.0167
389B	$\pm 2.100\times10^{-5}$	$\pm$ 0.0244	$\pm$ 0.0294	0.0538	0.1126
391D	$\pm 2.120\times10^{-5}$	$\pm$ 0.0113	$\pm$ 0.0137	-0.0137	0.0137
391B	$\pm 2.120\times10^{-5}$	$\pm$ 0.0124	$\pm$ 0.0150	0.0794	0.1094
392D	$\pm 2.094\times10^{-5}$	$\pm$ 0.0106	$\pm$ 0.0128	-0.0128	0.0128
392B	$\pm 2.094\times10^{-5}$	$\pm$ 0.0211	$\pm$ 0.0255	0.0641	0.1151

The uncertainties are reasonable and are small enough that mixture separation can still be observed in most cases. That is, the relation

$$0 \leq x_{distillate} < x_{feed} < x_{bottoms} < x_{azeotropic}, \quad \text{where } x_{azeotropic} = 0.11 \text{ mol/mol} \tag{10.5}$$

holds true for most experiments, even after allowing for the range in values caused by uncertainties. Alternatively, this can be expressed as, for most experiments:

$$x_{output,bottoms,max} > x_{output,bottoms,min} > x_{feed} \tag{10.6}$$

and

$$x_{output,distillate,min} < x_{output,distillate,max} < x_{feed} \tag{10.7}$$

The variation (or range) in x_{feed} (on the order of 10^{-5}) is negligible compared to the variation in x_{output} (on the order of 10^{-2}). This approximately thousand-fold difference in variation is because $w_{x_{feed}} \ll w_{x_{output}}$. The variable $w_{x_{output}}$ is relatively large because w_{ρ} is also relatively large. The uncertainty of the calculated density, w_{ρ}, can be decreased by using instruments of higher precision when measuring mass and volume, which are used to calculate ρ.

10.4 Distillation Conclusions and Recommendations

As shown by Table 10.1, the column separates the mixture adequately when the feed concentration is less than azeotropic ($x_{feed} < 0.11$). Feed concentrations greater than

azeotropic ($x_{feed} > 0.11$, or $c_{feed} > \sim 7.0$ mol/L) are not investigated since it would cause severe corrosion to the column, possibly rendering it inoperable for future experiments.

If the feed concentration is limited to $x_{feed} < 0.11$, then no relation is found between x_{feed} and the x_{output} (x_{output} refers collectively to $x_{distillate}$ and $x_{bottoms}$). As long as x_{feed} is any concentration less than azeotropic (0.11 mol/mol), $x_{distillate}$ tends to 0 mol/mol and $x_{bottoms}$ tends to 0.11 mol/mol. This is reasonable because the column is of sufficient height (see Section 7.2) to achieve the maximum possible degree of separation. The knowledge gained from the distillation experiments described in this thesis can be presently applied to the Cu-Cl cycle, in order to concentrate and recycle $HCl_{(aq)}$. By recycling $HCl_{(aq)}$, financial savings are realized. This constitutes a step toward optimization and integration.

To reinforce the knowledge gained by the experiments described in this thesis, it is recommended that another column be made from materials that do not corrode in the presence of HCl. Thus the output products (i.e., distillate and bottoms) would be free from corrosion and the errors caused by it. The results from the new column could be compared with the results given in this thesis, to quantify the errors caused by corrosion.

As shown in Table 10.4, the largest uncertainty occurs with concentration of the output product, that is $w_{x_{output}}$ is the largest uncertainty This, in turn, is due to the density, ρ, having a large uncertainty, w_ρ. Therefore, another recommendation to reinforce the knowledge gained by the experiments is to use instruments of higher precision and higher resolution when measuring the mass and volume to calculate output product density, ρ.

Furthermore, the availability and performance of various techniques (e.g., chemical analyzers, reagent strips) should be investigated to determine if there are feasible methods to directly measure HCl concentration.

At the time of the experiments described in this thesis, gages of the required sensitive are unavailable. An important future step is to use sensitive pressure gages on (i.e., the range of 0.04 kPa) to analyze the vapour phase (i.e., measure the vapour pressure) when the liquid phase is subcooled.

Another logical future step is to examine the heat duty to increase the energy efficiency of the column. The focus of this research is to examine the concentrations of the output, and little attention is paid to energy efficiency. (i.e., This research is for proof-of-concept, whereas further research on this topic would be for optimization and refinement).

Chapter 11

Conclusions and Recommendations

Conclusions and recommendations relating to distillation as well as those relating to the effect of metastability on crystallization are presented in this chapter.

$HCl_{(aq)}$ concentration via distillation, as well as the effect of metastability on $CuCl_{2(aq)}$ recovery via crystallization, are each important steps toward the optimization and integration of the Cu-Cl cycle. $HCl_{(aq)}$ concentration via distillation serves to decrease the operating cost of the cycle, because it recycles $HCl_{(aq)}$. Metastability has the effect of decreasing the thermal energy requirements of the Cu-Cl cycle because it decreases the precipitation temperature of $CuCl_{2(aq)}$ from $HCl_{(aq)}$ solutions.

Thus the objective of demonstrating the feasibility of increasing $HCl_{(aq)}$ concentration via distillation, as described in Chapter 1, is achieved. Also, the objective of investigating the relationship between cooling rate and MSZW for the crystallization of $CuCl_{2(aq)}$ from $HCl_{(aq)}$ solutions, as described in Section 4.2, is achieved.

Key findings are described as follows. The distillation system is found to separate the mixture as expected. The concentration of hydrogen chloride in the distillate is found to be less than that in the feed. The concentration of hydrogen chloride in the bottoms product is found to be greater than that in the feed, but less than azeotropic. However, the determination of hydrogen chloride concentration is hindered by corrosion product in the bottoms product. Please refer to Chapter 10 for a detailed analysis of the distillation results. MSZW is found to decrease with $HCl_{(aq)}$ concentration and to increase with cooling rate. A larger MSZW suggests a lower precipitation temperature, resulting in thermal energy savings. Please refer to Section 4.2.3 for a detailed analysis of the metastability results.

In order to obtain a more thorough understanding of $HCl_{(aq)}$ distillation, which in turn will help optimize the Cu-Cl cycle, it is recommended that further distillation experiments be performed at higher feed molarities. It is also recommended that corrosion ideally be prevented from occurring in the first place (i.e., by selecting non-reactive column materials), or, failing this, to more accurately determine the error in the calculation of concentration caused by the presence of corrosion product.

In order to obtain a more thorough understanding of the effect of metastability on the crystallization of $CuCl_{2(aq)}$ from $HCl_{(aq)}$ solutions, it is recommended that more sophisticated methods than the unaided eye be used to detect the onset of nucleation, which is the first step of crystal formation. This will result in more accurate determination of the precipitation temperature.

References

[1] Steam methane reforming. Student Energy. Accessed 28 June 2017. [Online]. Available: https://www.studentenergy.org/topics/steam-methane-reforming

[2] G. Naterer, S. Suppiah, L. Stolberg, M. Lewis, S. Ahmed, Z. Wang, M. Rosen, I. Dincer, K. Gabriel, E. Secnik, E. Easton, S. Lvov, V. Papangelakis, and A. Odukoya, "Progress of international program on hydrogen production with the copper-chlorine cycle," *International Journal of Hydrogen Energy*, vol. 39, pp. 2431–2445, 2014.

[3] M. Fayazuddin, "Challenges associated with separation of hcl-water azeotrope in copper-chlorine thermochemical hydrogen generation cycle (a case study)," Rajiv Gandhi Institute of Petroleum Technology, Rae Bareli, Tech. Rep., 2015.

[4] S. Aghahosseini, "System integration and optimization of copper-chlorine thermochemical cycle with various options for hydrogen production," Ph.D. dissertation, University of Ontario Institute of Technology, Oshawa, Ontario, Canada, 2013.

[5] R. Li, Q. Ye, X. Suo, X. Dai, and H. Yu, "Heat-integrated pressure-swing distillation process for separation of a maximum-boiling azeotrope ethylenediamine/water," *Chemical Engineering Research and Design*, vol. 105, pp. 1–15, 2016.

[6] Azeotrope / azeotropic mixture. Seperation Processes. Accessed 27 June 2017. [Online]. Available: http://www.separationprocesses.com/Distillation/DT_Chp01f.htm

[7] Misc distillation - azeotropic. Separation Processes. Accessed 27 June 2017. [Online]. Available: http://separationprocesses.com/Distillation/DT_Chp06c07.htm

[8] J. P. Knapp and M. F. Doherty, "A new pressure-swing distillation process for separating homogeneous azeotropic mixtures," *Ind. Eng. Chem Res.*, vol. 31, pp. 346–357, 1992.

[9] I. Chien, K. Zeng, and H. Chao, "Design and control of a complete heterogeneous azeotropic distillation column system," *Ind. Eng. Chem. Res.*, vol. 43, pp. 2160–2174, 2004.

[10] Misc distillation - extractive. Separation Processes. Accessed 31 March 2017. [Online]. Available: http://www.separationprocesses.com/Distillation/DT_Chp06d.htm

[11] Y. Wang, P. Cui, Y. Ma, and Z. Zhang, "Extractive distillation and pressure-swing distillation for thf/ethanol separation," *Journal of Chemical Technology and Biotechnology*, vol. 90, no. 8, pp. 1463–1472, 2015.

[12] R. Munoz, J. Monton, M. Burguet, and J. de la Torre, "Separation of isobutyl alcohol and isobutyl acetate by extractive distillation and pressure-swing distillation: Simulation and optimization," *Separation and Purification Technology*, vol. 50, no. 2, pp. 175–183, 2006.

[13] E. Lladosa, J. B. Monton, and M. C. Burguet, "Separation of di-n-propyl ether and n-propyl alcohol by extractive distillation and pressure-swing distillation: Computer simulation and economic optimization," *Chemical Engineering and Processing*, vol. 50, no. 11-12, pp. 1266–1274, 2011.

[14] E. Hosgor, T. Kucuk, I. N. Oksal, and D. B. Kaymak, "Design and control of distillation processes for methnaol-chloroform separation," *Computers and Chemical Engineering*, vol. 67, pp. 166–177, 2014.

[15] W. L. Luyben, "Comparison of extractive distillation and pressure-swing distillation for acetone/chloroform separation," *Computers and Chemical Engineering*, vol. 50, pp. 1–7, 2013.

[16] ——, "Comparison of extractive distillation and pressure-swing distillation for acetone-methanol separation," *Ind. Eng. Chem. Res.*, vol. 47, no. 8, pp. 2696–2707, 2008.

[17] Qvf - process systems: Concentration of hydrochloric acid above the azeotropic point. QVF. Accessed 6 May 2016. [Online]. Available: http://www.qvf.com/qvf-process-systems/mineral-acids/concentration-of-hydrochloric-acid.html

[18] A. Palomino, D. A. Parientes, H. Gomez, and P. Paucar, "Modelling ethanol-water pressure swing distillation in an structured packed bed column," *Rev. Per. Quim. Ing. Quim.*, vol. 16, no. 1, pp. 75–84, 2013.

[19] Y. Wang, Z. Zhang, D. Xu, W. Liu, and Z. Zhu, "Design and control of pressure-swing distillation for azeotropes with different types of boiling behavior at different pressures," *Journal of Process Control*, vol. 42, pp. 59–76, 2016.

[20] A. M. Fulgueras, J. Poudel, D. S. Kim, and J. Cho, "Optimization study of pressure-swing distillation for the separation process of a maximum-boiling azeotropic system of water-ethylenediamine," *Korean Journal of Chemical Engineering*, vol. 33, no. 1, pp. 46–56, 2016.

[21] J. R. Phimister and W. D. Seider, "Semicontinuous, pressure-swing distillation," *Ind. Eng. Chem. Res.*, vol. 39, pp. 122–130, 2000.

[22] G. Modla and P. Lang, "Feasibility of new pressure swing batch distillation methods," *Chemical Engineering Science*, vol. 63, no. 11, pp. 2856–2874, 2008.

[23] J.-U. Repke, A. Klein, D. Bogle, and G. Wozny, "Pressure swing batch distillation for homogenous azeotropic separation," *Chemical Engineering Research and Design*, vol. 85, no. 4, pp. 492–501, 2007.

[24] A. A. Kiss and Z. Olujic, "A review on process intensification in internally heat-integrated distillation columns," *Chemical Engineering and Processing*, vol. 86, pp. 125–144, 2014.

[25] H. Shahandeh, J. Ivakpour, and N. Kasiri, "Feasibility study of heat-integrated distillation columns using rigorous optimization," *Energy*, vol. 74, pp. 662–674, 2014.

[26] G. H. S. F. Ponce, M. M. J. C. Alves, F. R. Maciel, and M. M. R. Wolf, "Using an internally heat-integrated distillation column for ethanol-water separation for fuel applications," *Chemical Engineering Research and Design*, vol. 95, pp. 55–63, 2015.

[27] B. Kiran and A. K. Jana, "Assessing the performance improvement of an intensified heat integration scheme: Reactive pressure-swing distillation," *Applied Thermal Engineering*, vol. 76, pp. 509–520, 2015.

[28] J. F. Mulia-Soto and F.-T. Antonio, "Modeling, simulation and control of an internally heat integrated pressure-swing distillation process for bioethanol separation," *Computers and Chemical Engineering*, vol. 35, pp. 1532–1546, 2011.

[29] S. I. Abu-Eishah and W. L. Luyben, "Design and control of a two-column azeotropic distillation system," *Ind. Eng. Chem. Process Des. Dev.*, vol. 24, pp. 132–140, 1985.

[30] H. Cheng and W. L. Luyben, "Heat-integrated distillation columns for ternary separations," *Ind. Eng. Chem. Process Des. Dev.*, vol. 24, pp. 707–713, 1985.

[31] B. Kiran and A. K. Jana, "A hybrid heat integration scheme for bioethanol separation through pressure-swing distillation route," *Separation and Purification Technology*, vol. 142, pp. 307–315, 2015.

[32] J. P. Knapp, "Exploiting pressure effects in the distillation of homogeneous azeotropic mixtures," Ph.D. dissertation, UMI, Ann Arbor, 1991.

[33] J. Lee, J. Cho, D. M. Kim, and S. Park, "Separation of tetrahydrofuran and water using pressure swing distillation: Modeling and optimization," *Korean Journal of Chemical Engineering*, vol. 28, no. 2, pp. 1–15, 2011.

[34] G. Q. Wang, X. G. Yuan, and K. T. Yu, "Review of mass-transfer correlations for packed columns," *Industrial & Engineering Chemistry Research*, vol. 44, no. 23, pp. 8715–8729, 2005.

[35] G. M. Larin, V. V. Minin, B. V. Levin, and Y. A. Buslaev, "Complexation in the $CuCl_2$-HCl-H_2o system," *Bulletin of the Academy of Sciences of the USSR, Division of chemical science*, vol. 38, no. 6, pp. 1111–1116, 1989.

[36] P. Barrett and B. Glennon, "Characterizing the metastable zone width and solubility curve using lasentec FBRM and PVM," *Chemical Engineering Research and Design*, vol. 80, no. 7, pp. 799–805, 2002.

[37] W. B. Euler, L. Kirschenbaum, and B. Ruekberg, "Determination of k_{sp}, $\Delta G°$, $\Delta H°$, and $\Delta S°$ for the dissolution of calcium hydroxide in water a general chemistry experiment," *Journal of Chemical Education*, vol. 77, no. 8, pp. 1039–1040, 2000.

[38] X. Ni and A. Liao, "Effects of cooling rate and solution concentration on solution crystallization of L-glutamic acid in an oscillatory baffled crystallizer," *Crystal Growth & Design*, vol. 8, no. 8, pp. 2875–2881, 2008.

[39] J. E. Edwards, "Process modelling selection of thermodynamic methods," P & I Design, 2 Reed Street, Gladstone Industrial Estate, Thornaby, TS17 7AF, United Kingdom., Tech. Rep., 2008. [Online]. Available: https://www.chemstations.net/content/documents/Technical_Articles/thermo.pdf

[40] S. Hsieh, "Chemical process simulation - chemcad thermodynamic," Tech. Rep., 2008. [Online]. Available: web.thu.edu.tw/g96310005/www/6_thermo.pdf

[41] Metals and corrosion resistance. The Engineering ToolBox. Accessed 4 April 2017. [Online]. Available: http://www.engineeringtoolbox.com/metal-corrosion-resistance-d_491.html

[42] "Corrosion resistance of the austentic chromium-nickel stainless steels in chemical environments," INCO: The International Nickel Company, Inc., One New York Plaza, New York, N.Y. 10004, Tech. Rep., 1963. [Online]. Available: www.parrinst.com/files/Parr_Stainless-Steels-Corrosion-Info.pdf

[43] T. Bell. (2017) How to calculate the rate of metal corrosion. The Balance. Accessed 8 September 2017. [Online]. Available: https://www.thebalance.com/corrosion-rate-calculator-2339697

[44] (2000) Standard pipe schedules pipe sizes chart table data. Engineers Edge. Accessed 8 September 2017. [Online]. Available: http://www.engineersedge.com/pipe_schedules.htm

[45] "Product data sheet 316/316l stainless steel," AK Steel Corporation, 9227 Centre Pointe Drive, West Chester, OH 45069, Tech. Rep., 2007. [Online]. Available: www.aksteel.com/pdf/markets_products/stainless/austenitic/316_316l_data_sheet.pdf

[46] The complete aqueous hydrochloric acid solutions density-concentration calculator. handymath.com. Accessed 19 June 2017. [Online]. Available: http://www.handymath.com/cgi-bin/hcltble3.cgi?submit=Entry

[47] F. Tivadar, "Packed distillation columns," Budapest University of Technology and Economics - Faculty of Chemical Technology and Biotechnology, 2006. [Online]. Available: cuo2.kkft.bme.hu/packed.pdf

[48] E. Cussler, *Diffusion: Mass Transfer in Fluid Systems*, 3rd ed. New York: Cambridge University Press, 2007.

[49] R. Ellis, "Simple HETP calculation for distillation columns," *Chem. Eng. News*, vol. 31, p. 4163, 1953.

[50] M. E. Harrison and J. J. France, "Distillation column troubleshooting - part 2: Packed columns," *Chemical Engineering*, vol. 96, no. 4, p. 121, 1989.

[51] H. Z. Kister, *Distillation Design*. New York: McGraw-Hill, 1992.

[52] R. F. Strigle, *Packed tower design and applications : random and structured packings*, 2nd ed. Houston: Gulf Pub. Co., Book Division, 1994.

[53] M. J. Lockett, "Easily predict structured-packing HETPs," *Chemical Engineering Progress;*, vol. 94, no. 1, p. 60, 1998.

[54] T. B. Co. Ziegler-nichols method. Michigan Technological University. Accessed 15 May 2017. [Online]. Available: http://pages.mtu.edu/~tbco/cm416/zn.html

[55] *Datasheet NI 9472*, National Instruments, 5 2016. [Online]. Available: www.ni.com/pdf/manuals/373509b_02.pdf

[56] Inductors and calculus. All About Circuits. Accessed 23 March 2017. [Online]. Available: https://www.allaboutcircuits.com/textbook/direct-current/chpt-15/inductors-and-calculus/

[57] J. J. Fritz and C. R. Fuget, "Vapor pressure of aqueous hydrogen chloride solutions, 0° to 50°C," *Industrial and Engineering Chemistry*, vol. 1, no. 1, pp. 10–12, 1956.

[58] Wire color codes and limits of error. Omega. Accessed 24 May 2017. [Online]. Available: https://www.omega.ca/techref/colorcodes.html

[59] PB3002-S - documentation. Mettler Toledo. Accessed 24 May 2017. [Online]. Available: http://www.mt.com/ca/en/home/phased_out_products/others/PB3002-S.tabs.documents.html

[60] Errors and uncertainty. Paul Nicholls. Accessed 29 June 2017. [Online]. Available: http://pfnicholls.com/physics/Uncertainty.html

[61] Uncertainty analysis. SMU Lyle School of Engineering. Accessed 17 June 2017. [Online]. Available: http://lyle.smu.edu/me/2142/uncert/uncert.htm

Appendix A

Scripts

A.1 McCabe-Thiele Method

A MATLAB script that performs the McCabe-Thiele method and also calculates NTU for the Method of Transfer Units.

```
clear all; close all; clc;
% USER SET PARAMETERS
xb = 0.13;          %Bottoms composition [mole fraction HCl]
xf = 0.2232;          %Feed composition [mole fraction HCl]
xd = 0.99;          %Distillate (tops) [mole fraction HCl]
L = 0;              %Molar flow rate of reflux
D = 0.05;           %Molar flow rate of distillate
q = 0.999;          %Mole fraction of liquid in feed

x1 = 0:0.01:1;
data_name = 'xy_vle_100000Pa.xlsx';
y1 = transpose(xlsread(data_name,'E12:E112')); %Import Chemcad
    tabulated data from Excel
y = x1;                     %Equation of the y=x line
plot(x1,y1,'Color','r','LineWidth',4)     %Plot the VLE curve.
hold on
plot(x1,y,'Color',[0.6 0.6 0.6],'LineWidth',2)    %Plot the y=x
    line
axis ([0 1 0 1])
plot_title = title(data_name(1:end-5)); %The code (1:end-5)
    extracts a substring from the string data_name by removing the
    last 5 characters.
set(plot_title,'interpreter','none','FontSize',18)    %Changes the
    interpreter for the string plot_title so underscores are
    displayed as-is, and not as subscripts.
```

```
20 xlabel ('x_1 HCl Liquid Mole Fraction [-]','FontSize',18)
21 ylabel ('y_1 HCl Vapor Mole Fraciton [-]','FontSize',18)
22 set(gca,'TickDir','both','FontSize',16);
23 hold on
24
25 line([xb xb],[0 xb],'Color','k','LineWidth',2);   %Draw a line for
       the bottoms composition
26 line([xf xf],[0 xf],'Color','k','LineWidth',2);   %Draw a line for
       the feed composition
27 line([xd xd],[0 xd],'Color','k','LineWidth',2);   %Draw a line for
       the distillate composition
28
29 m_rec = L/(D+L);                    %Slope of rectifying line
30 b_rec = xd - m_rec*xd;               %Y-Intercept of rectifying line
31 rec_line = @(x) m_rec*x + b_rec;     %Equation of rectifying line
32 hold on
33
34 m_q = q/(q-1);               %Slope of q-line
35 b_q = xf - m_q*xf;           %Y-Intercept of q-line
36 q_line = @(x) m_q*x + b_q;   %Equation of q-line
37 hold on
38
39 intersection_x = (b_q - b_rec)/(m_rec - m_q);
40 intersection_y = m_rec*intersection_x + b_rec;
41
42 if isnan(intersection_x)            %Plot the rectifying line
43     fplot(rec_line,[0 xd],'Color','b','LineWidth',4)
44 else
45     fplot(rec_line,[intersection_x xd],'Color','b','LineWidth',4)
46 end
47
48
49 if isnan(intersection_x)    %Plot the q-line
50     fplot(q_line,[0 xf],'Color',[1 0.6 0],'LineWidth',4)
51 else
52     fplot(q_line,[min(intersection_x, xf),max(intersection_x, xf)],
           'Color',[1 0.6 0],'LineWidth',4)
53 end
54
55 line([xb intersection_x],[xb intersection_y],'Color','g','LineWidth
       ',4) %Draw the stripping line
56
57 m_s = (xb - intersection_y)/(xb - intersection_x);      %Slope of
       stripping line
```

```
58 b_s = xb - m_s*xb;                                          %Y-
       Intercept of stripping line
59 s_line = @(x) m_s*x + b_s;                                  %Equation
       of stripping line
60 fplot(s_line,[0 intersection_x])                            %Plot the
       stripping line
61
62 %Estimating the average slope of the VLE curve by taking the
       average slope
63 %of tangents at equal intervals.
64
65 n = 10; %Number of slope sample points
66 mi = zeros(1,n); %Pre-allocate array to increase speed and save
       memory.
67
68 for j = 1:n  %j is the loop index (loop counter)
69     a = int32(j*((length(x1)-1)/n));
70     mi(j) = (y1(a+1)-y1(a))/(x1(a+1)-x1(a));
71 end
72
73 mi;
74 ma = sum(mi(:))/length(mi)  %Display average slope of VLE curve.
75
76 %METHOD OF TRANSFER UNITS
77 yNTU = zeros(1,int32(100*xd-100*xb)); %Pre-allocate array to
       increase speed and save memory.
78
79 for j = int32(100*xb:100*xd)
80     if j < int32(100*intersection_x)
81         yNTU(j-int32(100*xb)+1) = s_line(x1(j+1));             %y-
               coordinate of stripping line (xb < x1 <=intersection_x)
82     elseif j >= int32(100*intersection_x+1)
83         yNTU(j-int32(100*xb)+1) = rec_line(x1(j+1));           %y-
               coordinate of rectifying line (intersection_x < x1 < 1)
84     end
85 end
86
87 deltay_NTU = y1(int32(100*xb):int32(100*xd)-1) - yNTU(1:end-1);
88 figure2 = figure;   %Plot figure to a new window.
89 yb = s_line(xb);
90 yd = rec_line(xd);
91 plot(y1(int32(100*xb):int32(100*xd)-1),1./deltay_NTU,'LineWidth'
       ,1.5)
92 % axis([yb yd 0 80])
```

```
93  title('Number of Transfer Units (NTU)','FontSize',18)
94  xlabel ('y','FontSize',20)
95  ylabel ('1/(y*-y)','FontSize',20)
96  set(gca,'TickDir','both','FontSize',20)
97  B = transpose(y1(int32(100*xb):int32(100*xd)-1)); % y1 represents
        the y*'s
98  C = transpose(yNTU); %yNTU represents the y's
99
100 yaxis = 1./deltay_NTU;
101 rectangle = zeros(1,length(yaxis));
102 for j = 1:length(yaxis)
103     rectangle(j) = yaxis(j)*((yd-yb)/length(yaxis));
104 end
105 NTU = sum(rectangle(:))
```

A.2 Method of Kline & McClintock

A MATLAB script that performs the method of Kline & McClintock.

```
clear
tic;
A =  xlsread('distillation_data.xlsx','OA_2','D37:AT52'); %Import
    data into matrix A.

% if(0)
%% 1) m_g [g]
syms m_full m_full_m_g
m_g(m_full,m_full_m_g) = m_full - m_full_m_g; %Define the function
    m_g.
d0 = diff(m_g,m_full);
d1 = diff(m_g,m_full_m_g);
w_m_g = zeros(size(A,1),1); %Initialize matrix, w_m_g, to store the
     uncertainties for m_g.
w_m_full = 0.01/2;          %Instrument uncertainty, given by
    manufacturer.
w_m_full_m_g = 0.01/2;      %Instrument uncertainty, given by
    manufacturer.
for i = 1:size(A,1)
     m_full = A(i,4);       %Get data from matrix A.
     m_full_m_g =  A(i,7);  %Get data from matrix A.
     %subs function allows for substitution of numerical values into
          symbolic expressions.
     w_m_g(i) = sqrt((subs(d0)*w_m_full)^2 + (subs(d1)*w_m_full_m_g)
         ^2); %vpa function converts from fractional to decimal
         representation.
end


%% 2) m_empty_average [g]
clear d0 d1 d2 d3       %Clearing undefined variables does not
    cause errors.
syms m_empty_1 m_empty_2 m_empty_3
m_empty_average(m_empty_1,m_empty_2,m_empty_3) = (m_empty_1 +
    m_empty_2 + m_empty_3)/3; %Define the function m_empty_average.
d0 = diff(m_empty_average,m_empty_1);
d1 = diff(m_empty_average,m_empty_2);
d2 = diff(m_empty_average,m_empty_3);
w_m_empty_average = zeros(size(A,1),1); %Initialize matrix,
    w_m_empty_average, to store the uncertainties for
```

```
    w_m_empty_average.
w_m_empty_1 = 0.01/2;                    %Instrument uncertainty,
    given by manufacturer.
w_m_empty_2 = 0.01/2;                    %Instrument uncertainty,
    given by manufacturer.
w_m_empty_3 = 0.01/2;                    %Instrument uncertainty,
    given by manufacturer.
for i = 1:size(A,1)
    m_empty_1 = A(i,1);     %Get data from matrix A.
    m_empty_2 = A(i,2);     %Get data from matrix A.
    m_empty_3 = A(i,3);     %Get data from matrix A.
    w_m_empty_average(i) = sqrt((subs(d0)*w_m_empty_1)^2 + (subs(d1
        )*w_m_empty_2)^2 + (subs(d2)*w_m_empty_3)^2); %vpa function
         converts from fractional to decimal representation.
end



%% 3) m_12MHCl [g]
clear d0 d1 d2 d3       %Clearing undefined variables does not
    cause errors.
syms m_H2O m_H2O_m_12MHCl
m_12MHCl(m_H2O,m_H2O_m_12MHCl) = m_H2O_m_12MHCl - m_H2O; %Define
    the function, m_12MHCl, by which the variable in question in
    calculated.
d0 = diff(m_12MHCl,m_H2O);
d1 = diff(m_12MHCl,m_H2O_m_12MHCl);
w_m_12MHCl = zeros(size(A,1),1);         %Define a matrix to store
    the uncertainties for the variable in question.
w_m_H2O = 0.01/2;                        %Instrument uncertainty,
    given by manufacturer.
w_m_H2O_m_12MHCl = 0.01/2;               %Instrument uncertainty,
    given by manufacturer.
for i = 1:size(A,1)
    m_H2O = A(i,5);             %Get data from matrix A.
    m_H2O_m_12MHCl = A(i,6);    %Get data from matrix A.
    w_m_12MHCl(i) = sqrt((subs(d0)*w_m_H2O)^2 + (subs(d1)*
        w_m_H2O_m_12MHCl)^2); %vpa function converts from
        fractional to decimal representation.
end


%% 4) v_12MHCl [ml]
```

```
59 clear d0 d1 d2 d3       %Clearing undefined variables does not
       cause errors.
60 syms m_12MHCl
61 v_12MHCl(m_12MHCl) = m_12MHCl/1.19;     %Define the function (i.e.,
        R) by which the variable in question in calculated.
62 d0 = diff(v_12MHCl,m_12MHCl);
63 w_v_12MHCl = zeros(size(A,1),1);        %Define a matrix to store
       the uncertainties for the variable in question.
64 for i = 1:size(A,1)
65     m_12MHCl = A(i,7);             %Get data from matrix A.
66     w_v_12MHCl(i) = sqrt((subs(d0)*w_m_12MHCl(i))^2); %vpa function
           converts from fractional to decimal representation.
67 end
68
69
70 %% 5) n_HClfeed [mol]
71 clear d0 d1 d2 d3       %Clearing undefined variables does not
       cause errors.
72 syms v_12MHCl
73 n_HClfeed(v_12MHCl) = 12*v_12MHCl/1000;     %Define the function (i
       .e., R) by which the variable in question in calculated.
74 d0 = diff(n_HClfeed,v_12MHCl);
75 w_n_HClfeed = zeros(size(A,1),1);        %Define a matrix to store
       the uncertainties for the variable in question.
76 for i = 1:size(A,1)
77     v_12MHCl = A(i,8);             %Get data from matrix A.
78     w_n_HClfeed(i) = sqrt((subs(d0)*w_v_12MHCl(i))^2); %vpa
           function converts from fractional to decimal representation
           .
79 end
80
81
82 %% 6) m_HClfeed [g]
83 clear d0 d1 d2 d3       %Clearing undefined variables does not
       cause errors.
84 syms n_HClfeed
85 m_HClfeed(n_HClfeed) = 36.46*n_HClfeed;     %Define the function (i
       .e., R) by which the variable in question in calculated.
86 d0 = diff(m_HClfeed,n_HClfeed);
87 w_m_HClfeed = zeros(size(A,1),1);        %Define a matrix to store
       the uncertainties for the variable in question.
88 for i = 1:size(A,1)
89     n_HClfeed = A(i,9);             %Get data from matrix A.
```

```
90      w_m_HClfeed(i) = sqrt((subs(d0)*w_n_HClfeed(i))^2); %vpa
            function converts from fractional to decimal representation
            .
91  end
92
93
94  %% 7) m_H2Ofeed [g]
95  clear d0 d1 d2 d3       %Clearing undefined variables does not
        cause errors.
96  syms m_H2O_m_12MHCl m_HClfeed
97  m_H2Ofeed(m_H2O_m_12MHCl,m_HClfeed) = m_H2O_m_12MHCl - m_HClfeed;
            %Define the function (i.e., R) by which the variable in
        question in calculated.
98  d0 = diff(m_H2Ofeed,m_H2O_m_12MHCl);
99  d1 = diff(m_H2Ofeed,m_HClfeed);
100 w_m_H2Ofeed = zeros(size(A,1),1);        %Define a matrix to store
        the uncertainties for the variable in question.
101 for i = 1:size(A,1)
102     m_H2O_m_12MHCl = A(i,6);            %Get data from matrix A.
103     m_HClfeed = A(i,10);            %Get data from matrix A.
104     w_m_H2Ofeed(i) = sqrt((subs(d0)*w_m_H2O_m_12MHCl)^2 + (subs(d1)
            *w_m_HClfeed(i))^2); %vpa function converts from fractional
             to decimal representation.
105 end
106
107
108 %% 8) n_H2Ofeed [mol]
109 clear d0 d1 d2 d3       %Clearing undefined variables does not
        cause errors.
110 syms m_H2Ofeed
111 n_H2Ofeed(m_H2Ofeed) = m_H2Ofeed/18.02;     %Define the function (i
        .e., R) by which the variable in question in calculated.
112 d0 = diff(n_H2Ofeed,m_H2Ofeed);
113 w_n_H2Ofeed = zeros(size(A,1),1);        %Define a matrix to store
        the uncertainties for the variable in question.
114 %m_H2Ofeed = A(:,11);
115 for i = 1:size(A,1)
116     m_H2Ofeed = A(i,11);            %Get data from matrix A.
117     w_n_H2Ofeed(i) = sqrt((subs(d0)*w_m_H2Ofeed(i))^2); %vpa
            function converts from fractional to decimal representation
            .
118 end
119
120
```

```
121 %% 9) x_feed [mol/mol]
122 clear d0 d1 d2 d3       %Clearing undefined variables does not
        cause errors.
123 syms n_HClfeed n_H2Ofeed
124 x_feed(n_HClfeed,n_H2Ofeed) = n_HClfeed/(n_HClfeed + n_H2Ofeed);
          %Define the function (i.e., R) by which the variable in
        question in calculated.
125 d0 = diff(x_feed,n_HClfeed);
126 d1 = diff(x_feed,n_H2Ofeed);
127 w_x_feed = zeros(size(A,1),1);        %Define a matrix to store the
         uncertainties for the variable in question.
128 for i = 1:size(A,1)
129     n_HClfeed = A(i,9);             %Get data from matrix A.
130     n_H2Ofeed = A(i,12);             %Get data from matrix A.
131     if (n_H2Ofeed ~= 0)
132         w_x_feed(i) = sqrt((subs(d0)*w_n_HClfeed(i))^2 + (subs(d1)*
                w_n_H2Ofeed(i))^2); %vpa function converts from
                fractional to decimal representation.
133     end
134 end
135
136
137 %% 10) rho [g/ml]
138 clear d0 d1 d2 d3       %Clearing undefined variables does not
        cause errors.
139 syms m_sample v_sample
140 rho(m_sample,v_sample) = m_sample/v_sample;     %Define the
        function (i.e., R) by which the variable in question in
        calculated.
141 d0 = diff(rho,m_sample);
142 d1 = diff(rho,v_sample);
143 w_rho = zeros(size(A,1),1);        %Define a matrix to store the
        uncertainties for the variable in question.
144 %m_H2Ofeed = A(:,11);
145 w_m_sample = 0.0001/2;          %Instrument uncertainty, given by
        manufacturer.
146 w_v_sample = 0.2/2;             %Instrument uncertainty, given by
        manufacturer.
147 for i = 1:size(A,1)
148     m_sample = A(i,32);             %Get data from matrix A for
            subbing into the partial derviatives.
149     v_sample = A(i,33);             %Get data from matrix A for
            subbing into the partial derviatives.
```

```
150     w_rho(i) = sqrt((subs(d0)*w_m_sample)^2 + (subs(d1)*w_v_sample)
            ^2); %vpa function converts from fractional to decimal
            representation.
151 end
152
153
154 %% 11) x_output [mol/mol]
155 clear d0 d1 d2 d3       %Clearing undefined variables does not
        cause errors.
156 syms rho T
157 x_output(rho,T) = (rho-1.013+(5.057*10^-4)*T)/0.8283;     %Define
        the function (i.e., R) by which the variable in question in
        calculated.
158 d0 = diff(x_output,rho);
159 d1 = diff(x_output,T);
160 w_x_output = zeros(size(A,1),1);        %Define a matrix to store
        the uncertainties for the variable in question.
161 %m_H2Ofeed = A(:,11);
162 w_T = 1;          %Instrument uncertainty, given by manufacturer.
163 for i = 1:size(A,1)
164     rho = A(i,34);          %Get data from matrix A for subbing
            into the partial derviatives.
165     T = A(i,31);            %Get data from matrix A for subbing
            into the partial derviatives.
166     w_x_output(i) = sqrt((subs(d0)*w_rho(i))^2 + (subs(d1)*w_T)^2);
             %vpa function converts from fractional to decimal
            representation.
167 end
168
169
170 % end
171
172 titles = {'w_m_empty_average', 'w_m_12MHCl', 'w_v_12MHCl', '
        w_n_HClfeed', 'w_m_HClfeed', 'w_m_H2Ofeed', 'w_n_H2Ofeed', '
        w_x_feed','w_rho','w_x_output'};
173 w = [w_m_empty_average, w_m_12MHCl, w_v_12MHCl, w_n_HClfeed,
        w_m_HClfeed, w_m_H2Ofeed, w_n_H2Ofeed, w_x_feed, w_rho,
        w_x_output];
174 uncertainties = [titles; num2cell(w)];
175
176
177 TimeSpent = toc;
```

Appendix B

Crystallization Results

Experiments are performed in which heated solutions of $CuCl_2$ dissolved in various molarities of $HCl_{(aq)}$ are prepared and cooled through a temperature range. Table B.1 summarizes the results of these experiments (i.e., whether or not crystals were formed).

Table B.1: Crystallization Results

$\mathbf{m_{CuCl_2}}$ **[g]**	$\mathbf{HCl_{(aq)}}$ **Conc. [mol/L]**	**Range [°C]**	**Result**
45.4	6	60-20	Successful - Crystallization occurred
33.5	7	20-0	Successful - Crystallization occurred
19.4	9	20-0	Successful - Crystallization occurred
58.3	3	20-0	Successful - Crystallization occurred (also paste formed)
38.0	7	60-20	Successful - Crystallization occurred
32.1	7	20-0	Paste formed
38.2	7	60-20	Successful - Crystallization occurred (also paste formed)
45.4	6	60-20	Successful - Crystallization occurred
29.8	8	60-20	Successful - Crystallization occurred
25.2	8	20-0	Successful - Crystallization occurred
22.6	7	60-20	No stirring while pouring HCl or after Solids in bottom of reactor (i.e., 2 insoluble components (solid at bottom, liquid above)) WG13 contains liquid pipetted from top portion of reactor, Remained as the aforementioned 2 phases, Oven @ 80°C

22.7	9	60-20	FAILED - paste formed Did not get to add $HCl_{(aq)}$
23.0	9	60-20	FAILED - Too much $CuCl_2$ added to liquid water, Precipitate formed, Did not get to add $HCl_{(aq)}$
19.0	9	20-0	Insoluble precipitate first observed at approximately 5℃near reactor bottom, Re-dissolved upon re-heating
40.3	12	20-0	FAILED - Did not crystallize, Remained liquid, Temperature decreased as low as 1℃
38.9	6	20-0	Success - Semi-crystalline paste formed after adding HCl, No stirring while pouring HCl or after
38.5	6	20-0	FAILED - paste formed
23.0	9	60-20	Stayed liquid, did not crystallize
40.0	3	20-0	FAILED - Did not crystallize
30.0	3	20-0	FAILED - Did not crystallize
46.8	6	60-20	FAILED - Did not crystallize
39.8	6	60-20	FAILED - paste formed
39.8	6	60-20	Successful - Crystallization occurred
50.2	3	20-0	Successful - Crystallization occurred
54.6	3	60-20	Successful - Crystallization occurred
60.28	3	60-20	FAILED - Did not crystallize
67.3	3	60-20	FAILED - Did not crystallize
79.8	3	20-0	FAILED - Did not crystallize, Paste formed
80.0	0	20-0	FAILED - Did not crystallize
57.6	0	20-0	FAILED - Did not crystallize
80.0	0	20-0	FAILED - Did not crystallize
60.78	3	20-0	FAILED - Did not crystallize
60.78	3	20-0	FAILED - Did not crystallize